Stony Brook University

The official electronic file of this thesis or dissertation is maintained by the University Libraries on behalf of The Graduate School at Stony Brook University.

Biotinylated self-assembled micelles as potential vehicles for targeted anti-cancer drug

delivery

A Thesis Presented

by

Weiyi Li

to

The Graduate School

in Partial Fulfillment of the

Requirements

for the Degree of

Master of Science

in

Materials Science and Engineering

Stony Brook University

August 2015

Stony Brook University

The Graduate School

Weiyi Li

We, the thesis committee for the above candidate for the

Master of Science degree, hereby recommend

acceptance of this thesis.

Yizhi Meng – Thesis Advisor

Assistant Professor, Materials Science and Engineering

Dilip Gersappe – Committee Member

Professor & Graduate Program Director, Materials Science and Engineering

Jian Cao – Committee Member

Professor, School of Medicine

This thesis is accepted by the Graduate School

Charles Taber

Dean of the Graduate School

Abstract of the Thesis

Biotinylated self-assembled micelles as potential vehicles for targeted anti-cancer drug

delivery

by

Weiyi Li

Master of Science

in

Materials Science and Engineering

Stony Brook University

2015

Chemotherapy is one of the most commonly used cancer treatments. However, many side effects could occur due to the non-specific bindings of extremely toxic anti-cancer drugs to healthy cells and organs. Targeted delivery has been developed to enhance the selectivity of drug delivery vehicle and minimize side effects of chemotherapy. In this study, the hydrophobically modified glycol chitosan (HGC) micelle was further modified with a biotin-avidin-biotin (B-A-B) strategy to improve the tumor-selective ability of HGC. Firstly, HGC was biotinylated either at the amine groups (NH_2) or the hydroxyl groups (OH) on the chitosan main chain. Then the biotin-4-fluorescein, as a model biomolecule, was linked to biotinylated HGC via the strong and specific biotin-avidin linkage. A near-infrared fluorescent dye cyanine 5.5 was also conjugated to the amine groups on HGC for the additional visualization of HGC micelles. The hydrodynamic diameters of these two types of nanoparticles were 197.9 ± 6.4 nm (NH_2-conjugated) and 173.6 ± 3.8 nm (OH-conjugated), and their surface charges were 20.3 ± 2.1 mV (NH_2-conjugated)

and 12.0±1.2 mV (OH-conjugated), ensuring the enhanced permeability and retention (EPR) effect of nanoparticles and their interactions with negatively charged cancer cells membranes. Both types of nanoparticles were delivered at a concentration of 0.3 mg/mL to the 4T1 mouse breast cancer cells. Confocal microscope images showed that nanoparticles were distributed evenly throughout the cytoplasm of cancer cells after 6 hours of exposure. Co-localization of the Cy5.5 and FITC signals further confirmed the formation of BHGC-A-B4F structure.

Table of Contents

List of Figures

List of Tables

List of Abbreviations

HGC   Hydrophobically modified glycol chitosan

BHGC   Biotinylated HGC

B4F   Biotin-4-fluorscein

FITC   Fluorescein

Cy5.5   Cyanine 5.5

DMSO   Dimethyl sulfoxide

DAPI   4',6-diamidino-2-phenylindole

HABA   4'-hydroxyazobenzene-2-carboxylic acid

DCC   Dicyclohexylcarbodiimide

DMAP   4-dimethylaminopyridine

EDC   1-Ethyl-3-(3-dimethylaminopropyl)carbodiimide

Sulfo-NHS   N-hydroxysulfosuccinimide

PBS   Phosphate-buffered saline

Acknowledgements

The person I would like to thank first is my advisor Dr. Yizhi Meng. She has provided me precious guidance and academic support for my studies. Her dedication to research and enthusiasm for life will always inspire me. Thank you for encouraging me and making me feel warm inside in these two years.

I express my sincere gratitude to the members of my committee. I am especially thankful to Dr. Jian Cao for his scientific knowledge and insightful comments. I would also thank Dr. Dilip Gersappe for his support and suggestion.

I would like to express my thanks to Shelagh Zegers from the school of Marine and Atmospheric Sciences for her kindly technical assistance with lyophilization. I am thankful to Dr. Dmytro Nykypanchuk at Center for Functional Nanomaterials of Brookhaven National Laboratory for the experiment instrument training.

Many thanks to my lab colleagues Giulia Suarato and Derek Rammelkamp for their assistances. They introduced me to nanoparticles and helped me a lot for the cell work, nanoparticles synthesis and confocal microscope. I want to express my warmest gratitude to them for their care and kindness.

Last but not least, I would like to thank my parents, Jiashu Li and Yan Li. They worked so hard to support my life and study here. You are the very source of my strength.

Chapter 1: Introduction

1.1 Cancer therapy

Cancer is known as the abnormal cell proliferation caused by interaction between the genetic and environmental factors.[1] It is the second leading cause of death in the U.S.A. The estimated deaths for colon cancer, lung cancer and breast cancer in 2014 are 50,310, 159,260 and 40,430, respectively. [2]

While cancer incidence rate remains stable, the survival rate has increased, rising from 49% in 1970s to 68% in 2010s. This improvement can be attributed to the advancement in cancer diagnosis and treatment. [2] Besides traditional cancer therapies such as chemotherapy, surgery and radiation therapy, targeted therapy has been developed.

1.1.1 Chemotherapy

Chemotherapy is a cancer treatment that destroys tumors by interfering cancer cells mutation with cytotoxic drugs or other substances. There are many different types of chemotherapy drugs, which can be categorized by how they work. For example, doxorubicin (DOX) is an antibiotics drug that kills cancer cells by interfering enzymes involved in DNA replication. Paclitaxel (PTX), as a mitotic inhibitor, is able to stabilize cellular microtubules and hence prevent cancer cell division.

Although chemotherapy is effective in killing rapidly dividing cells and decreasing the risk of recurrence of tumor after surgery, we should be aware of its side effects. Most commonly used cytotoxic drugs for chemotherapy are non-specific. They are also toxic to normally dividing cells and tissues especially for bone marrow constituents, resulting in severe side effects like kidney damage, teratogenicity and immunosuppression. For example, febrile neutropenia caused by the suppression of bone marrow can be life threatening. [3] During chemotherapy treatment, some patients may become resistant to certain drugs. To overcome this resistance, a few types of drugs are usually given in combination, which may further lead to the phenomenon of multidrug resistance (MDR). [4] It is the insensitivity of tumor cells to a variety of anticancer drugs. For instance, breast cancer, colorectal cancer, pancreatic cancer and gastric cancer are found to be resistant to antimetabolites drugs like 5-FU and methotrexate; colorectal and small-cell lung carcinoma have shown resistance to topoisomerase I inhibitors such as irinotecan. [5] Currently, some hypotheses have been proposed for MDR: the alteration in target expression, altered drug transportation through cell membranes or increased DNA repair. [5] Generally, MDR behavior associates with two or more factors. While many patients feel scared of the side effects of conventional chemotherapy, targeted therapy has been drawing considerable attention with its high efficacy as well as low toxicity to normal cells and organs.

1.1.2 Targeted therapy

Targeted therapy is a novel technology that successfully combines chemotherapy with nanotechnology. Unlike traditional chemotherapy, targeted therapy delivers drug to tumor site selectivity by encapsulating the anti-cancer drug in certain vehicles.

Nanoparticle (Np) is one of the potential candidates for drug delivery. It shows promise in cancer treatment as the unique structure of solid tumor allows Np to preferentially accumulate at tumor site. Due to the rapid division, tumor cells always need more oxygen and nutrients applied by the enhanced vascular permeability and impaired lymphatic system. [6] This defective architecture leads to prolonged circulation and accumulation of drugs in tumor area via the passive "enhanced permeability and retention (EPR) effect". Since cytotoxic drugs are encapsulated inside delivered Nps, their toxicities to normal cells can be minimized. Clinically approved EPR-based drugs include Nab-paclitaxel (paclitaxel bonded to albumin), DaunoXome® (liposomal daunorubicin) and so on.

In addition to passive targeting, active targeting can be achieved by modifying the Nps surfaces with affinity ligands aiming at specific receptors such as Her2/neu, epidermal growth factor and folate that are overexpressed on tumor cells. For example, cyclic arginine-glycine-aspartic (RGD) peptide has been conjugated to the poly (ethylene glycol)-*b*-poly (2-(diisopropyl amino) ethylmethacrylate) copolymer to image the angiogenic tumor endothelial cells by binding to $\alpha_V\beta_3$ integrins. [7] On epithelial cells and normal endothelial cells, $\alpha_V\beta_3$ integrins are expressed at a low level, but on angiogenic tumor endothelial cells, they are always overexpressed. Clinically, non-small cell lung cancer drugs Tarceva® (erlotinib) and Iressa® **(**gefitinib) act by specifically targeting the overactive epidermal growth factor receptor (EGFR) tyrosine kinase on tumors.

The size of the nanoparticles plays an important role in their interactions with the cells. It has been reported that particles with diameters larger than 200 nm might activate the human complement system and therefore being most likely cleared by the reticuloendothelial system

(RES) (e.g. Kupffer cells in the liver). For intravenous administration, particles with diameters in the range of 100 to 200 nm show decreased rate of clearance with the enhanced permeability and retention effect, attaining an extended circulation time in human body. [8] Since relatively large particle size is necessary to load sufficient amount of drugs, here nanoparticles usually refer to colloidal systems ranging in diameter from 50 nm to 0.1 μm.

1.2 Micelles

Many materials have been exploited as targeted Nps such as polymeric nanoparticles, [9] dendrimers, [10] metallic nanoparticles, [11] semiconductor nanoparticles (quantum dots) [12] and liposome. [13] With various hydrophobicities, surface charges, particle sizes and other physiochemical properties, these materials are selected for the delivery of different types of drugs, proteins, or genes. In recent years, polymeric micelles have attracted an increasing interest. Under appropriate aqueous environment, amphiphilic block copolymer is able to self-assemble to a shell-core structure above the critical micelle concentration. (Figure 1)

For regular micelle, a hydrophobic core-hydrophilic shell structure is formed in hydrophilic solvent when its polar moiety orients to the solvent and the non-polar part moves away from the solvent. In contrast, when exposed to a hydrophobic solvent, reverse micelle forms a hydrophilic core with hydrophobic portion aligned towards the solvent. [14] Compared with conventional surfactant micelles, polymeric micelles are thermodynamically more stable. [15]
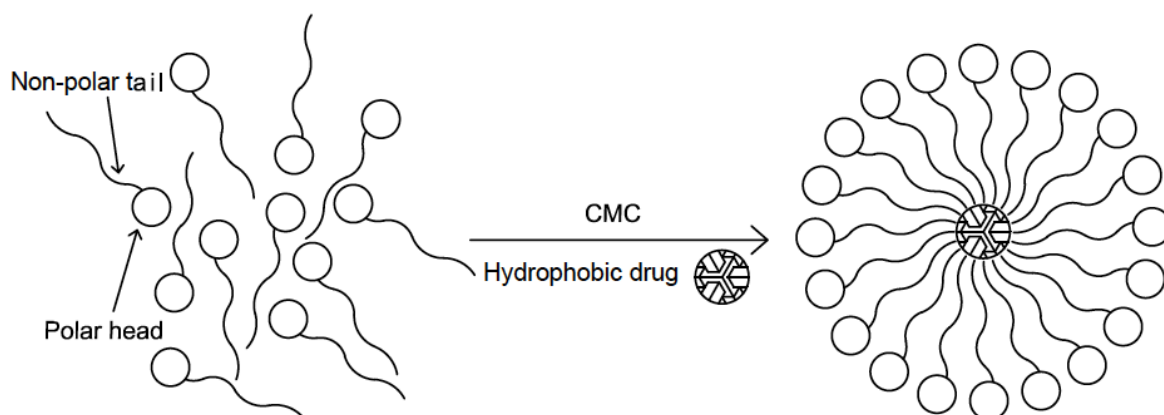
Figure 1.Schematic depicting the formation of regular micelle after reaching critical micelle concentration (CMC).

Reverse micelle is a potential candidate to deliver hydrophilic drugs and proteins. A. Miller et al. [16] synthesized a block copolymer poly(ε-caprolactone)-block-poly(2-vinyl pyridine) (PCL-*b*-P2VP). The highest loading efficiency for proteins ovalbumin and bovine serum albumin in PCL-*b*-P2VP was 7.8% (wt%) and the release of ovalbumin from this micellar system in oleic acid could be sustained for 12-30 hours, demonstrating PCL-*b*-P2VP was a potential delivery agent for proteins.

Clinically, many anticancer drugs show poor solubilities in aqueous environment such as doxorubicin (DOX), paclitaxel (PTX) or camptothecin (CPT), and therefore they can be encapsulated in the hydrophobic core of a micelle with the hydrophilic shell to prevent the core from interacting with the environment. Forrest et al. developed poly(ethylene glycol)-*b*-(ε-caprolactone) (PEG-*b*-PCL) micellar system as a carrier for PTX prodrug PAX7'C$_6$. [17] This polymeric micelle showed diameter less than 50 nm while being able to load 17-22% (w/w%) prodrug. The *in vitro* release of PAX7' from PEG-*b*-PCL was sustained up to 14 days.

A lipid-functionalized dextran micelle was designed for the delivery of DOX by E. Kobayashi's group. [18] Doxorubicin (DOX) is an anthracycline antibiotic widely used to treat blood cancer, breast cancer, lung cancer and many other types of cancer. In Kobayashi's study, the DOX encapsulated in micelles showed a 5- to 10 -fold higher antiproliferative activity than free DOX in osteosarcoma and SKOV-3 ovarian cancer cell lines. [18] In addition, micelles encapsulating DOX exhibited greater antiproliferative activities at lower concentration in both DOX-sensitive and DOX-resistant cancer cell lines. The lower dose promised fewer side effects in patients.

Similar to dextran, other natural polysaccharides including starch, alginate [19], pullulan [20] and chitosan [19] have been exploited as potential materials to prepare micellar systems in drug delivery application due to their excellent biocompatibilities, biodegradabilities and abundant resources. Moreover, the large number of functional groups on their long chains makes it easy to modify polysaccharides with various hydrophobic moieties like linoleic acid, stearic acid and cholanic acid, leading to flexible derivatives.

1.3 Chitosan-based nanoparticles as drug carriers

Chitosan is a copolymer of β-(1-4)-linked D-glucosamine and N-acetyl-D-glucosamine derived by deacetylation of natural chitin (Figure 2). As the only naturally cationic polysaccharide, chitosan exhibits great mucoadhesive properties, which increases its contact with absorbing mucosa, resulting in prolonged drug penetration time. [21] Moreover, as a biomaterial, the antimicrobial activity of chitosan has been observed against a wide variety of microorganisms including fungi, algae and some bacteria. [22] This inherent antimicrobial

property of chitosan decreases the risk of infection inside human body. [23] However, unmodified chitosan is only soluble in acidic environments of pH below 6.5. The poor solubility in neutral solutions limits its application as a drug vehicle.
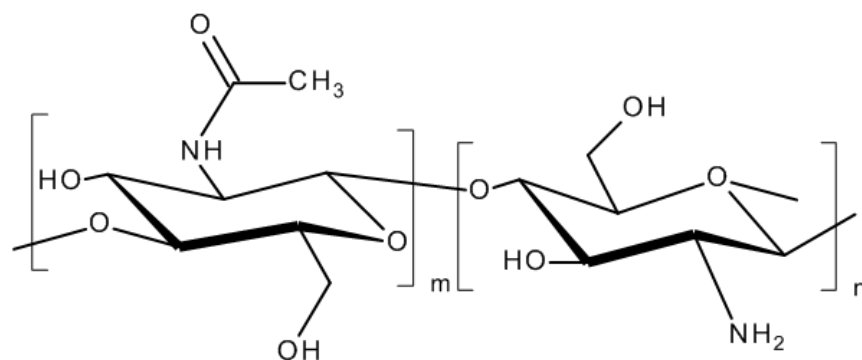
Figure 2. Chemical structure of chitosan.

1.3.1 Chemical modification of chitosan

The barrier of low solubility of chitosan can be overcome with chemical modification. Glycol chitosan (GC), for example, is a hydrophilic chitosan derivative achieved by introducing ethylene glycol group to the insoluble chitosan. It is a useful ingredient for the synthesis of functional chitosan-based micelles. Huo et al. developed N-octyl-O-glycol chitosan (OGC) by introducing hydrophobic alkyl chains to glycol chitosan backbone. As a carrier for PTX, OGC showed a high drug loading capacity (32 wt.%). The critical micelle concentration of OGC in water determined to be was 5.3-32.5 mg/mL, which further confirmed the formation of micelle. [24] Compared with free PTX, PTX encapsulated in OGC micelle caused less hemolysis and hypersensitivity.

Kwon's group [25] successfully synthesized 5β-cholanic acid hydrophobically modified glycol chitosan (HGC) with the amide bond between glycol chitosan and 5β-cholanic acid, mediated with crosslinker N-(3-Dimethylaminopropyl)-N'-ethylcarbodiimide hydrochloride (EDC) and N-hydroxysulfosuccinimide (Sulfo-NHS). As a natural derivative of bile acid, 5β-cholanic acid plays an important role for the emulsification, solubilization and uptake of cholesterol, fats and lipophilic acid in human body. [26] HGC has been proved as an efficient carrier of various poorly soluble anticancer drugs including paclitaxel [27], camptothecin [28], protein [29] and peptide [30], exhibiting its promising future in drug delivery application. Park et al. [30] loaded fluorescein isothiocyanate (FITC) labeled RGD (tripeptide arginine-glycine-aspartic that can specifically bind to the tumor marker-$\alpha_v\beta_3$ integrin) into HGC. The diameter of this micelle ranged from 189 nm to 265 nm, varying with the feed ratio of FITC-RGD to HGC. The peptide loading efficiency was higher than 75% and FITC-RGD could be cumulatively released from HGC for up to 1 day in PBS buffer. Also, cell adhesion and migration assays demonstrated that the binding of RGD peptide to $\alpha_v\beta_3$ integrins was not be impaired by fluorescent labeling. The selectivity of HGC-based drug delivery system could hence be enhanced by modifying the nanoparticles with cell-specific recognition molecules.

1.3.2 Safety of chitosan

Chitosan is widely considered as being non-toxic since it is biodegradable and biocompatible. In the United States, chitosan has been sold as a dietary supplement for years. However, it has not been approved by the US Food and Drug Administration (FDA) for drug delivery until now. [31] Due to the haemolytic activity, more than 50 mg/kg/day intravenous

injection of chitosan in rabbits could induce blood cell aggregation and cause death. [32] The toxicity of chitosan is highly related to the degree of deacetylation, molecular weight and chemical modification. M. Huo et al. developed N-octyl-O-glycol chitosan (OGC) nanoparticles for the delivery of paclitaxel. [24] The cell viability study against human hepatoma HepG2 cells showed that unloaded OGC micelles did not exhibit any toxicity even at a very high concentration of 10 μg/mL. This study demonstrated that the safety of chitosan could be improved by surface modifications.

Different from animal-derived chitosan, fungal chitosan is derived from chitin found in cell walls of fungi instead of exoskeleton of crustaceans and is considered to be safer for biomedical applications from an allergenic point of view. [23] In all, the safety of chitosan and its derivatives should always be emphasized in biomedical studies.

1.4 Biotin-avidin interaction

The (strept)-avidin-biotin system forms a strong non-covalent bond ($K_d \approx 10^{-15}$M) and has been widely utilized in a variety of applications. For example, in protein detection, biotinylated primary or secondary antibodies can be detected with a biotinylated protein labeled with fluorescent or enzymatic detection reagents via the avidin-biotin binding. [33] In addition, the biotin-avidin interaction can be used for selective drug delivery to overcome the non-specific binding and increase drug accumulation at the targeted area. Avidin is a glycoprotein found in egg white. Its bacterial counterpart streptavidin, is located from *Streptomyces avidinii,* showing

similar properties to avidin. As a tetrameric protein, avidin has four identical subunits, each binding to one biotin molecule with high affinity and specificity. [34]

1.4.1 Biotinylation reagents

Biotin (vitamin H) plays an important role in human body by assisting in various metabolic reactions related to amino acids and carbohydrates. It is an ideal candidate for labeling of proteins and macromolecules because of its relatively small molecular weight (244 Da) and valeric acid side chain. It is possible, therefore, to conjugate reactive moieties to biotin without interfering the avidin-biotin binding. For example, commercially available biotinylation reagents including amine-reactive biotin, sulfhydryl-reactive biotin, carbonyl- or carboxyl- reactive biotin, photo-reactive (non-selective) biotin and hydrogen-reactive biotin can be easily conjugated to biomolecules with corresponding functional groups. Moreover, the solubility and spacer arm length of a biotinylation reagent can be modified. By adding a poly(ethylene glycol) (PEG) spacer arm, the solubility of a biotinylation agent will be increased, allowing the reaction in hydrophilic environment. The length of spacer arm of a biotinylation reagent influences its ability to bind to avidin. The availability of biotin for binding to avidin can be improved by elongating the spacer arm. Adding or removing chemical groups between biotin and the functional side chain is a flexible way to change the spacer arm length e.g. Sulfo-NHS-LC-biotin. (Figure 3) [35]
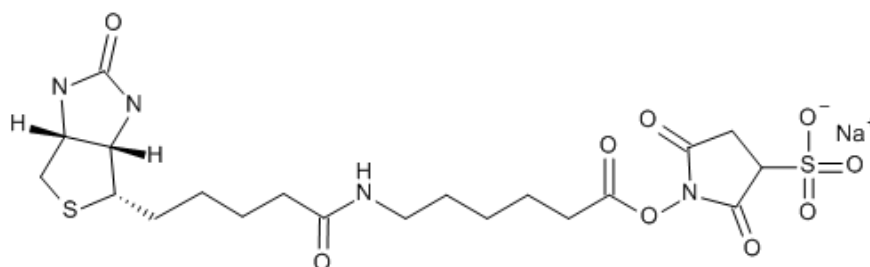
Figure 3. Chemical structure of Sulfo-NHS-LC-biotin.

1.4.2 Biotin-avidin complex

As one of the strongest non-covalent bonds, the avidin-biotin binding is a useful tool for preparing a "sandwich" complex between two biotinylated reagents. For instance, M. Tarrus's group assembled a RGD-equipped avidin with biotinylated TNF-related apoptosis-inducing ligand (TRAIL). [36] RGD peptide was first introduced to avidin via a poly(ethylene glycol) linker. Then, the complex of biotinylated TRAIL with RGD-PEG-avidin was formed through the biotin-avidin interaction. (Figure 4) The experiment result showed that this complex was able to bind to the tumor maker $\alpha_v\beta_3$ integrins and killed tumor cells by inducing apoptosis.
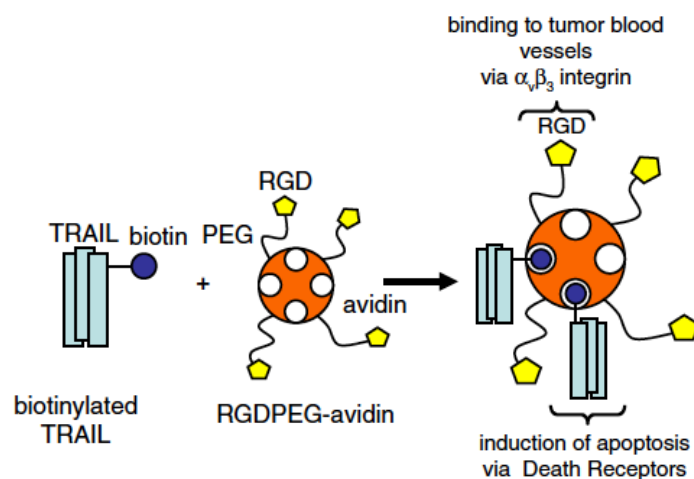
Figure 4. Schematic representation for synthesis of RGD-avidin/TRAIL complexes. [36]

The unique site targeting ability of biotinylated chitosan paves the way for its application in biotechnology fields. For instance, poly(ethyleneimine) (PEI) had been conjugated to biotinlyated chitosan as a gene carrier. [37] Also, J. P. Liu et al. [38] designed lectin-conjugated chitosan nanoparticles. Firstly, chitosan and lectin were biotinylated respectively with NHS-biotin by forming an amide bond between NHS ester and their amine groups. After that, biotinylated lectin was linked to biotinylated chitosan through the biotin-avidin interaction. The atomic force microscope (AFM) study showed that the lectin-conjugated chitosan nanoparticles were in a spherical shape with a particle size between 100 nm and 200 nm.

1.4.3 HABA assay

HABA (4- hydroxyazobenzene-2-carboxylic acid) assay is a reliable and convenient method to determine the degree of biotinylation. HABA-avidin complex shows a maximum absorption at the wavelength of 500 nm (A_{500}). When a biotin-conjugated molecule is added to

12

HABA/avidin mixture, the A_{500} will decrease in proportion with the amount of biotin molecules since biotin displaces HABA with its higher affinity to avidin. Therefore, the biotinylated level of the sample can be evaluated with the change in light absorbance.

1.4.4 B4F quenching assay

B4F (biotin-4-fluorescein) is a biotin-fluorescein conjugate with an ethylene diamine spacer synthesized by G. Kada's group. [39] B4F is a biotin-carboxy fluorescein conjugate with ethylene diamine as a 4-atom spacer. It has been shown that compared with conventional fluorescein biotin, biotin-4-fluorescein binds to avidin or streptavidin much faster. [40] Because of the short space between fluorescein and biotin, B4F usually suffers from highly quenching ($\geq$ 80%) upon binding to avidin or streptavidin. The strong fluorescence quenching association with the B4F could be attributed to the large decrease in the extinction coefficient of B4F at 493 nm upon binding to avidin. [41]

As a result, B4F has been widely applied to sensitively quantify the available (strept)-avidin in solutions. Specifically, the amount of biotin-binding sites can be determined by titrating a serial dilution of B4F to a known amount of avidin-conjugated molecules.

1.4.5 Avidin and biotin for tumor targeting

Biotin is one of the most common cancer cell recognition molecules. It has been shown that biotin receptors are overexpressed on some cancer cells surfaces because tumor cells need extra biotin to sustain their rapid divisions than normal cells. [42] M. Li's group developed

biotin-decorated fluorescent silica nanoparticles to image cytoplasm tumor cells with overexpressed biotin receptors. This biotin-conjugated nanoparticles exhibited strong light emission when delivered to cervical carcinoma HeLa and hepatocellular carcinoma BEL-7402 cell lines, demonstrating its ability to selectively image cancer cells. [36]

Moreover, avidin also shows certain tumor-targeted properties. L. Bu et al. loaded the same amount of anti-cancer drugs *trans*-resveratrol in biotin modified chitosan nanoparticles (B-CS-NPs) and biotin/avidin modified chitosan nanoparticles (A-B-CS-NPs). It turned out that both systems had higher inhibitory rates towards human liver cancer cells HepG2 than free *trans*-resveratrol drugs while the nanoparticles with additional avidin modification was more cytotoxic against HepG2 cells than chitosan with only biotin modification. This phenomenon could probably be explained by avidin's ability to bind to lectins, a type of cell-surface protein involved in interfering cell-cell interaction. [43]

1.5 Fluorescent probe

Fluorescent probe has been extensively applied in biomedical imaging. This technology images the object within a defined light bandwidth with a highly sensitive CCD detector. For biological investigations, the emission wavelength of fluorescent probe always ranges from 190 to 1100 nm, covering optical spectrum to near infrared region (NIR). [44] Conjugating or encapsulating NIR probe to nanoparticles is a popular non-invasive method to visualize particles distribution inside body or particular cells.

Commonly used fluorophores in biomedical fields include fluorescein isothiocyanate (FITC), Alexa Fluor, Dylight Fluor, rhodamine, cyanine, 4',6-diamidino-2-phenylindole (DAPI),

coumarin etc. These dyes have various properties such as binding mechanism, absorption and excitation wavelength and should be chosen depending on real experiment conditions and type of the instrument in use. A variety of fluorophore conjugated molecules are commercially available. Fluorescent labeled (strept)-avidin and fluorescent labeled biotin are widely used in life science research for fluorescent detection. For example, a biotinylated antibody bound to protein can be detected with fluorescent labeled avidin via the avidin-biotin interaction. Or, the delivery of micelle composed of fluorescent avidin can be tracked by using microscope facilities.

Cyanine is a group of NIR probes owning polymethine portions, which are made up from an odd number of CH groups bound together by alternating single and double bonds. [45] It was firstly synthesized in last century and still being broadly used today. Unlike visible probes, NIR probe can penetrate in to body and tissue for several centimeters without toxicity and absorption by hemoglobin or water, making it feasible for *in vivo* study. [46] K. Kim et al. [47] labeled tumor homing chitosan-based nanoparticles with Cyanine5.5 (Cy5.5) and successfully monitored the fate of nanoparticles *in vivo*. This methodology provides an effective and non-invasive way to evaluate the performance of drug delivery system.

1.6 Characterization of nanoparticles

There are many methods to characterize a nanoparticles system. The commonly used techniques include dynamic light scattering (DLS), zeta potential analyzer and proton-nuclear magnetic resonance (NMR). A brief introduction of these three techniques will be given here.

DLS is a technique to analyze hydrodynamic size and size distribution of small molecules in solutions. Macromolecules in solution are undergoing Brownian motion, so when light hits molecules, the intensity of scattered light will fluctuate over time by changing constructive or destructive interference. This fluctuation is then recorded by a fast photon counter, giving hydrodynamic diameter of the sample.

Electrical charge is a crucial property for particles used in pharmaceutical applications. It influences the interactions between biomolecules with targeted cells. For example, with the unique cationic property, chitosan is able to bind to negatively charged epithelial cell surfaces, facilitating its penetration into cells cytoplasm. [48] The zeta potential of a particle surface can be derived from the measurement of its velocity in suspension undergoing electrophoresis. This measurement is conducted by using phase analysis light scattering (PALS).

Commercially available DLS instruments combine particle size and zeta potential analyzers. They can be used to determine the size and zeta potential on a wide variety of materials. For example, the size of the N-octyl-O-glycol chitosan prepared by M. R. Huo was in the range of 190.7 nm to 228.3 nm and zeta potential was between 30.2 mV to 24.6 mV, detected with DLS and zeta potential. This result demonstrated N-octyl-O-glycol chitosan was cationic and suitable for drug delivery application. [24]

Proton-NMR identifies the ^{1}H nuclei of a compound in a magnetic field. It is a very useful technique to exploit the structure of a substance. In a lot of studies [24][25][27][37], Proton-NMR spectra were obtained to confirm the chemical conjugations of nanoparticles.

Chapter 2: Objective

Biofunctionalizing the surfaces of drug delivery vehicles with cell-specific recognition molecules is widely utilized to enhance the selectivity of delivery system. Hydrophobically modified glycol chitosan (HGC) has been shown to be a potential candidate for the delivery of hydrophobic anti-cancer drugs and has also demonstrated high cytocompatibility and rapid uptake by both osteosarcoma and breast cancer cells. [49] The main objective of this study therefore is to examine the physicochemical characteristics and delivery efficiency of HGC-based nanoparticles that have been modified for target-selectivity. We hypothesized that the avidin-biotin binding system can be used to attach a biomolecule of interest to the HGC micelle.

To test our hypothesis, we: (1) prepared HGC-based nanoparticles via the biotin-avidin-biotin binding, (2) characterized the physiochemical properties of nanoparticles and (3) studied their uptake in a model cell line.

<u>Aim 1:</u> Two strategies were used to biotinylate either glycol chitosan or HGC: Either D-(+)-biotin was covalently conjugated to the hydroxyl (-OH) groups on HGC to prepare the O-type nanoparticles or Sulfo-NHS-LC-biotin was added to the amine ($-NH_2$) groups on GC (glycol chitosan) to prepare the N-type nanoparticles. Biotinylated GC or Biotinylated HGC was then avidinylated and B4F was added as a model molecule via the avidin-biotin interaction. HGC micelles were labeled with near-infrared fluorescent dye Cyanine 5.5 to aid in the visualization of their intracellular distribution in cultured cancer cells.

Aim 2: HABA assay was performed to analyze the biotinylation level of biotinylated HGC (O-type) or biotinylated glycol chitosan (N-type). To confirm the conjugation of avidin on biotinylated glycol chitosan, B4F quenching assay was conducted, giving the amount of biotin-binding sites on the surface of BGC-A. The hydrodynamic diameters and surface charge of the nanoparticles were measured with the Dynamic Light Scattering and zeta potential.

Aim 3: Cellular uptake of HGC-based micelles was studied in 4T1 mouse breast cancer cells, which were treated with nanoparticles at a concentration of 0.3 mg/mL for up to 6 hours. Treated cells were then mounted on glass sides and imaged under a confocal microscope. The localization and uptake of nanoparticles were visualized in the FITC and Cy5.5 channels for biotin-4-fluorescein and Cy5.5, respectively.

Chapter 3: Materials and Methods

3.1 Materials

Glycol chitosan (250kDa molecular weight, degree of deacetylation $\geq$ 60% (titration)), 5β-cholanic acid, N-hydroxysuccinimide sodium salt (Sulfo-NHS), Triton X-100 solution, 37% in H$_2$O formaldehyde solution, 1-Ethyl-3- (3-dimethylaminopropyl) carbodiimide hydrochloride (EDC) and 4-(Dimethylamino)pyridine (DMAP) were purchased from Sigma-Aldrich (St. Louis, MO). HABA (4'-hydroxyazobenzene-2-carboxylic acid)/avidin assay, Sulfo-NHS-LC-Biotin, avidin from egg white and Alexa Fluor®546 phalloidin were purchased from Thermo Fisher Scientific(Rockford, IL). Monoreactive hydroxysuccinimide Cyanine 5.5 (Cy5.5 NHS ester) was purchased from Lumiprobe (Hallandale Beach, FL). Biotin-4-fluorescein (B4F) was obtained from Biotium (Hayward, CA). D-(+)-Biotin and N,N′-Dicyclohexylcarbodiimidewas (DCC) were purchased from Santa Cruz Biotechnology (Dallas, Texas). Anhydrous dimethyl sulfoxide (DMSO) was purchased from EMD Chemicals (Darmstadt, Germany). The 4T1 murine mammary carcinoma cell line was purchased from the American Type Culture Collection (Manassas, VA). Serum-free, phenol red-free Dulbecco's Modified Eagle Media (DMEM) was obtained from Gibco (Carlsbad, CA).

3.2 Nanoparticles synthesis

In this study, biotin was conjugated to glycol chitosan by two different methods. In the first method, D-(+)-biotin molecules were covalently linked to the hydroxyl (-OH) groups on the hydrophobically modified glycol chitosan (HGC) micelles. Nanoparticles prepared this way are referred to as "O-type". In the second method, Sulfo-NHS-LC-biotin molecules were added to the amine ($-NH_2$) groups on glycol chitosan. This type of nanoparticles is named as "N-type" since Sulfo-NHS-LC-biotin was conjugated to the $-NH_2$ groups. The detailed synthesis procedures are described in Section 3.2.1 (formation of O-type nanoparticles) and Section 3.2.2 (formation of N-type nanoparticles).

3.2.1 Formation of O-type nanoparticles

In this method, glycol chitosan was first modified with 5β-cholanic acid to form the hydrophobically modified glycol chitosan (HGC). Then, D-(+)-biotin molecules were covalently linked to the hydroxyl (-OH) groups on HGC micelles. Finally, biotinylated fluorescein (B4F) was linked to the micelles via biotin-avidin binding as a model molecule. The synthesis of O-type nanoparticles flow chart is shown in Figure 5.
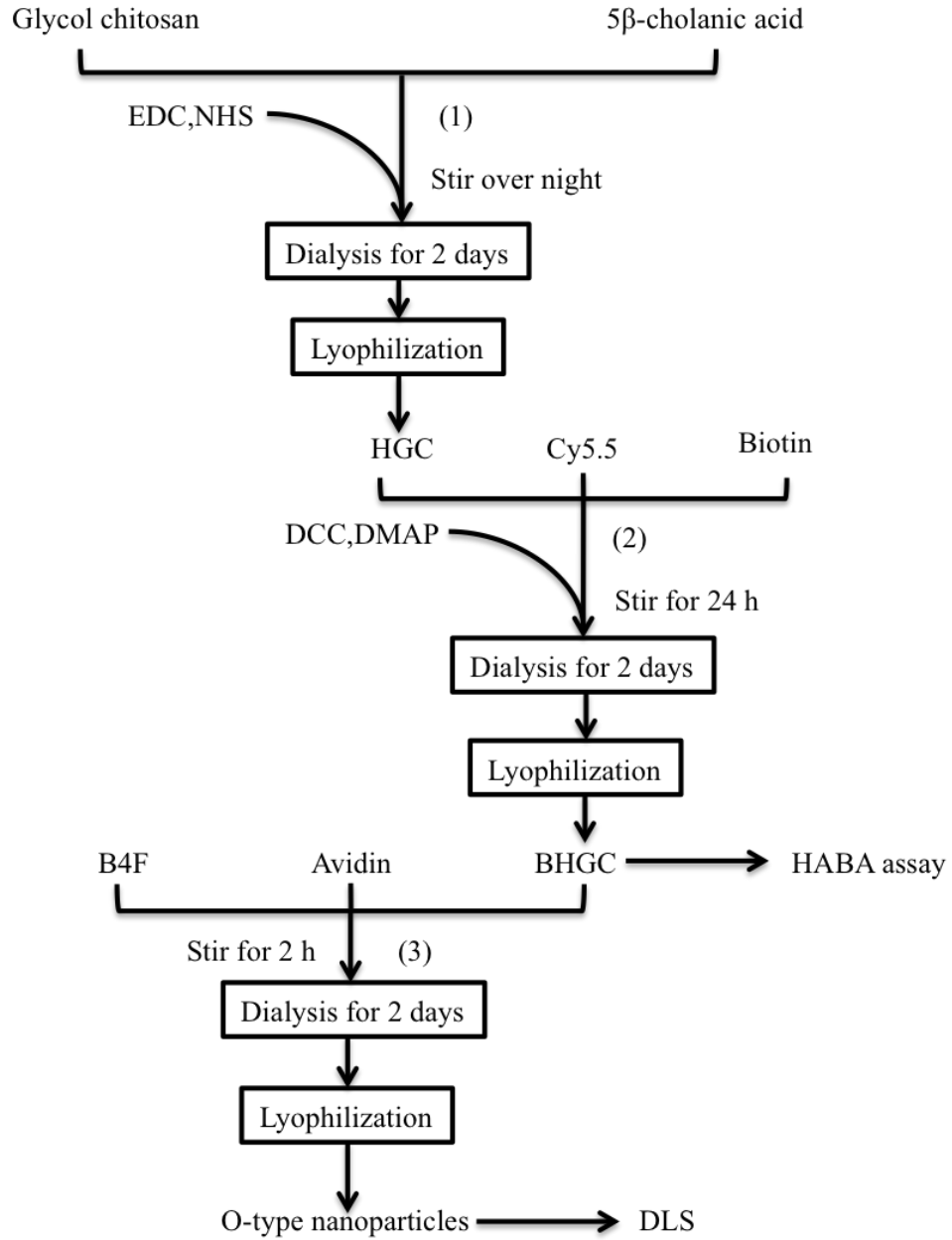
Figure 5. Synthesis of O-type nanoparticles (Cy5.5-labeled biotinylated hydrophobically modified glycol chitosan-avidin-biotin-4-fluorescein) flow chart.

3.2.1.1 Hydrophobic modification of glycol chitosan

The hydrophobic modification of glycol chitosan was achieved via the formation of an amide bond between glycol chitosan and 5β-cholanic acid (Figure 6) (see Figure 5 step (1)). Specifically, 500 mg of glycol chitosan was first dissolved in 60 mL of HPLC water and 100 mg of 5β-cholanic acid was dissolved in 60 mL of methanol. Then 1.5 molar equivalents of Sulfo-NHS (72 mg) and EDC (120 mg) were added to the 5β-cholanic solution to activate the carboxylic groups. The glycol chitosan and 5β-cholanic acid solutions were then mixed in a 250 mL beaker and stirred overnight at room temperature. To remove the unconjugated 5β-cholanic acid, EDC and Sulfo-NHS, the reactant mixture was dialyzed with 10 kDa molecular weight cut off (MWCO) dialysis cassettes (Slide-A-lyzer, Thermo Scientific, Waltham, MA) against a water/methanol mixture (1:4 v/v) for 1 day and then against HPLC water for another day. The media was changed 2 times per day. After dialysis, the mixture was centrifuged at 2790 rpm for 30 minutes and then lyophilized (Freeze Zone Plus Benchtop Freeze Dry System, Labconco, Kansas City, MO).
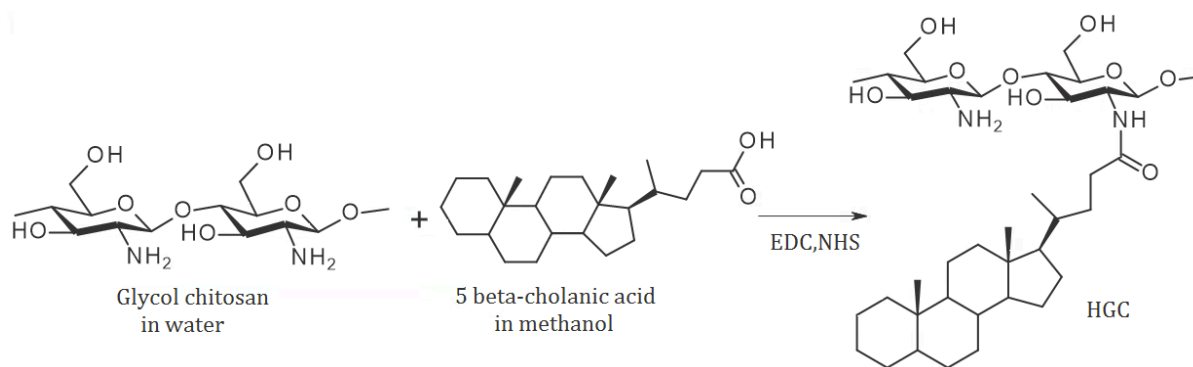
Figure 6. Schematic depicting the synthesis of hydrophobically modified glycol chitosan (HGC).

3.2.1.2 Coupling of biotin to HGC

The D-(+)-biotin was coupled to HGC via DCC and DMAP mediated Steglich esterification (Figure 7) (see Figure 5 step (2)). Specifically, 100 mg of HGC was suspended in 40 mL of anhydrous DMSO and dissolved by stirring overnight. Then, 11 mg of biotin was added to 20 mL of anhydrous DMSO and the carboxylic groups were activated by adding 40 mg of DCC and 25 mg of DMAP. The biotin solution was then mixed with HGC solution and reacted for 24 hours at room temperature to allow the reaction between activated carboxyl on biotin and hydroxyl groups on HGC. Since DCC was moisture-and oxygen-sensitive, the reaction was carried out under a nitrogen atmosphere. Afterwards, 1 mg of Cyanine 5.5 NHS ester was added to label the HGC. After 24 hours, the reactant mixture was dialyzed against HPLC water for 3 days with 10K MWCO dialysis cassettes to remove unreacted DCC, DMAP and biotin. The water was changed twice a day. After dialysis, the mixture was washed with 100% ethyl alcohol 3 times and re-dissolved in water to remove DMSO from sample before lyophilization.
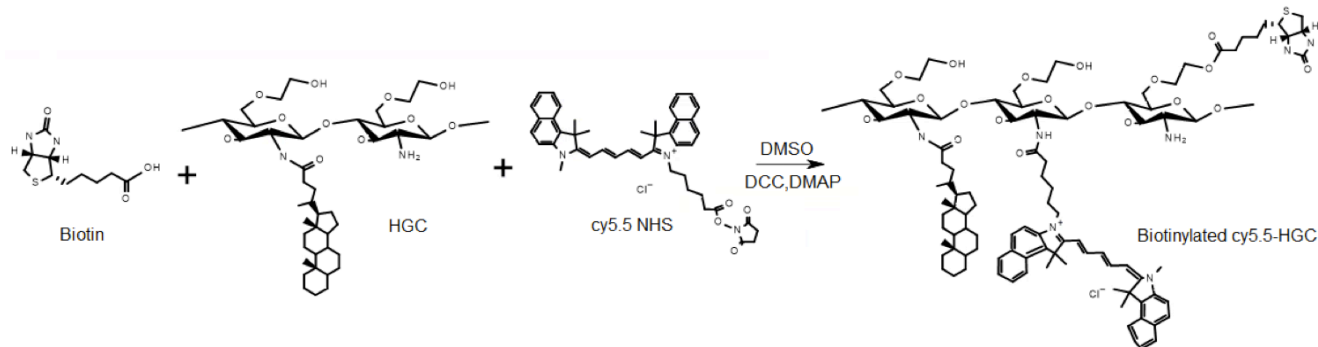
Figure 7. Schematic depicting the synthesis of Cy5.5 labeled biotinylated HGC.

3.2.1.3 Determination of the level of biotinylation for O-type nanoparticles

The HABA/avidin assay was used to quantitate biotinylation following manufacturer's instructions. [50] Briefly, 160 μL of PBS was added to a 96-well microplate (Thermo Scientific, Waltham, MA) and 20 μL of the HABA/Avidin premixed standard solution was added to each well. To ensure even mixing, the microplate was placed on an orbital shaker for 2 minutes. The absorbance at 500 nm was measured with a spectrophotometer (Tecan Infinite® 200 PRO, Tecan, Switzerland). Afterwards, the lyophilized O-type nanoparticles was re-dissolved in PBS and 20 μL of 1mg/mL of nanoparticles solution was added to each well. Absorbance was measured at 500 nm. The amount of biotin on biotinylated hydrophobically modified glycol chitosan (BHGC) was derived from the difference in the measured absorbance ($\Delta A500$) as shown from Equation 1 to Equation 3, where 34,000 ($M^{-1}cm^{-1}$) is the extinction coefficient of HABA/avidin samples at 500 nm and 0.5 (cm) is the light path of the sample in 96-well microplate. The biotinylation efficiency was calculated with Equation 4:

$$mmol\ BHGC\ per\ mL = \frac{BHGC\ concentration\ (mg\,/\,mL)}{Molecular\ weight\ of\ BHGC\ (mg\,/\,mmol)} \quad (1)$$

$$\frac{mmol\ biotin}{mL\ solution} = \frac{\Delta A_{500}}{(34,000*0.5)} \quad (2)$$

$$mmol\ of\ biotin\ per\ mmol\ of\ BHGC = \frac{mmol\ biotin}{mmol\ BHGC\ per\ mL*mL\ solution} \quad (3)$$

$$Biotinylation\ effciency = \frac{mmol\ of\ biotin\ per\ mmol\ of\ BHGC}{molar\ ratio\ of\ biotin\ added\ to\ BHGC} \quad (4)$$

3.2.1.4 Avidinylation of O-type nanoparticles

Avidin was then bound to the O-type nanoparticles through the avidin-biotin binding (see Figure 5 step (3)). Specifically, 15 mg of the biotinylated HGC (BHGC) was dissolved in 20 mL of DMSO and 1 molar equivalent of avidin (5 mg) was added to the BHGC solution.

3.2.1.5 Introduction of the B4F model molecule to O-type nanoparticles

The B4F was introduced to the O-type nanoparticles through the interaction between biotin on B4F and avidin (see Figure 5 step (3)). After adding the avidin to BHGC and stirring for 2 hours, 0.2 mg of B4F was dissolved in DMSO and added dropwise under magnetic stirring. After 2 hours, the reactant mixture was loaded into the 10 kDa MWCO dialysis cassettes and dialyzed against HPLC water for 2 days. The mixture was then lyophilized. Lyophilized O-type nanoparticles were grinded into a fine powder with mortar and pestle.

3.2.2 Formation of N-type nanoparticles

In this method, Sulfo-NHS-LC-biotin molecules were first added to the amine ($-NH_2$) groups on glycol chitosan. Biotinylated glycol chitosan was then hydrophobically modified with 5β-cholanic acid to form self-assembled nanomicelles and subsequently linked with B4F after avidinylation. The synthesis of N-type nanoparticles flow chart is shown in Figure 8.
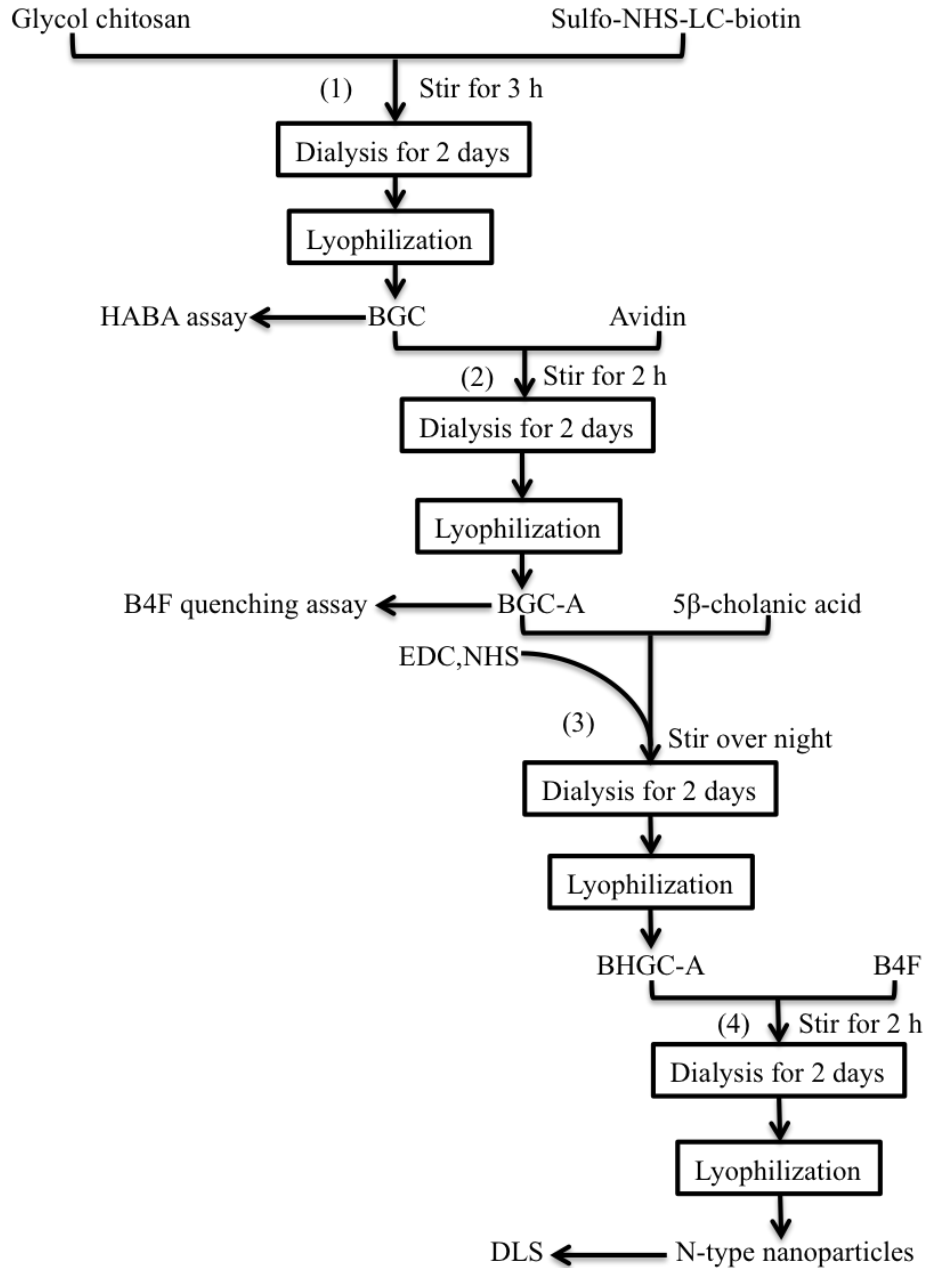
Figure 8. Synthesis of N-type nanoparticles (Cy5.5-labeled biotinylated hydrophobically modified glycol chitosan-avidin-biotin-4-fluorescein) flow chart.

3.2.2.1 Coupling of Sulfo-NHS-LC-biotin to HGC

The biotinylated glycol chitosan (BGC) was synthesized via the reaction between the NHS ester on Sulfo-NHS-LC-biotin and the amine on glycol chitosan (Figure 9) (see Figure 8 step (1)). Specifically, 300 mg of glycol chitosan was suspended in 45 mL of water and dissolved completely via magnetic stirring. Various amounts of Sulfo-NHS-LC-biotin (10-15 mg) was also dissolved in water and added dropwise to the glycol chitosan solution. The reaction took place at room temperature for 3 hours, after which, the reactant mixture was dialyzed against HPLC water for 2 days with 10kDa MWCO dialysis cassettes. The media was changed twice a day and the solution was lyophilized. The biotinylation level of BGC was determined with HABA assay as described in Section 3.2.1.3.
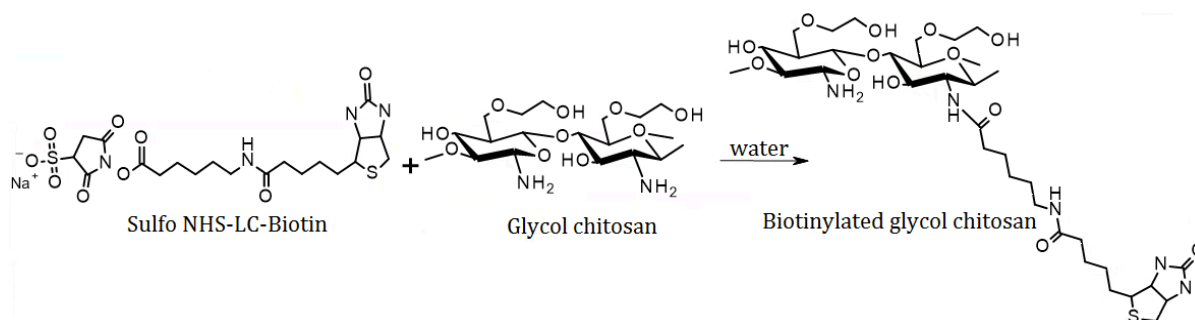
Figure 9. Schematic depicting the biotinylation of glycol chitosan (BGC).

3.3.2.2 Avidinylation of N-type nanoparticles

The N-type nanoparticles were avidinylated with a similar method as described in section 3.2.1.4 (see Figure 8 step (2)). Biotin density on the surface of the avidinylated BGC (BGC-A) was analyzed with the HABA/avidin (see Section 3.2.1.3) and B4F quenching assays.

3.2.2.3 B4F fluorescence quenching assay

The biotin-4-fluorescein (B4F) quenching assay was applied to characterize the amount of biotin-binding sites per BGC-A. In a UV-transparent flat-bottom 96-well microplate, 100 μL of 1 nM BGC-A was titrated in triplicate with 100 μL of a 2-fold serial B4F dilution from 0 and 0.244 nM to 500 nM. Samples were incubated in dark for 1 hour at room temperature. Afterwards, 100 μL of 1 nM BGC were titrated with 100 μL of B4F with the same method as the control group with no biotin-binding site. A row of the serial dilution of B4F alone was prepared as the positive control group. The fluorescence intensity was measured using the Tecan microplate reader at 523 nm (emission) with the excitation wavelength of 496 nm. The biotin binding sites is determined by the point of intersection between two binding regimes in the titration profile of B4F (see Figure 10). Since the B4F fluorescence quenches by binding to avidin molecules, there are two binding regimes occur in the titration profile. [51] For avidin, the first regime at low B4F concentration is nonlinear and a second linear regime occurs after all four sites of avidin are occupied by B4F. The saturation point, defined as the intersection point in Figure 10, demonstrating the biotin-binding sites on avidinylated compounds.
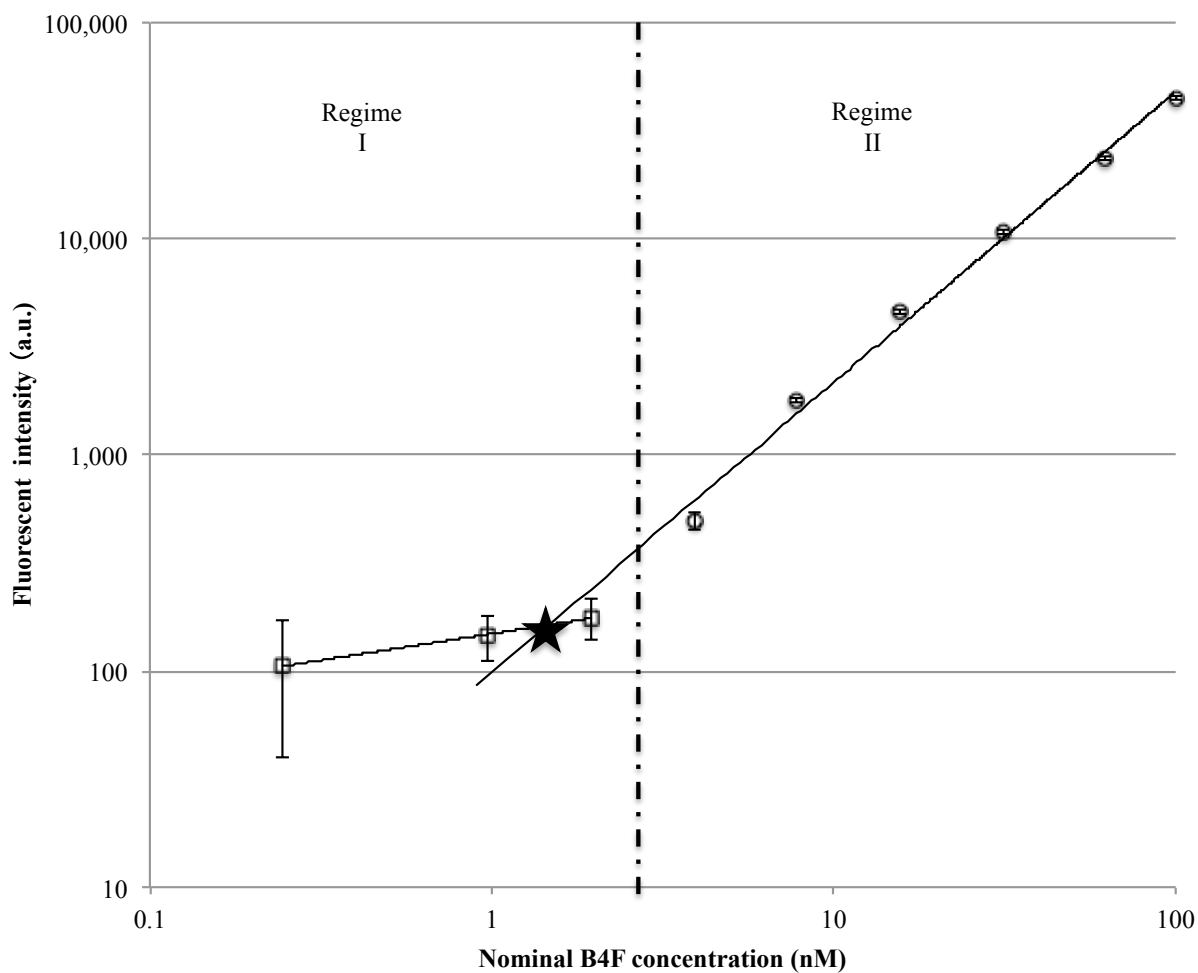
Figure 10. Representative log-log B4F titration profile. Regime I (open rectangle) at lower B4F concentration was fit to a second-order polynomial; regime II (open circle) at higher B4F concentration was fit to a linear model function. The number of biotin-binding sites is determined by the point of intersection (saturation point) between two regimes, indicated by the star.

3.2.2.4 Hydrophobic modification of N-type nanoparticles

The hydrophobic modification of N-type nanoparticles was obtained by the same strategy as described in Section 3.2.1.1 (see Figure 8 step (3)). Here the 5β-cholanic acid was bound to the primary amino group on BGC-A under the mediation of EDC and NHS.

3.2.2.5 Introduction of the B4F model molecule to N-type nanoparticles

The N-type nanoparticles were firstly labeled with the near-infrared dye Cy5.5. Model molecule B4F was then introduced to the N-type nanoparticles via the avidin-biotin interaction (see Figure 8 step (4)). Specifically, 50 mg of the N-type nanoparticles were first dissolved in 20 ml of DMSO, and 0.5 mg of Cy5.5 dissolved in 100 μL DMSO and were added dropwise under magnetic stirring. The reactant mixture was shielded from light. After 6 hours, 0.5 mg of B4F in DMSO was added drop wise to the mixture and continued stirring for 2 hours. The mixture was loaded into the 10 kDa MWCO dialysis cassettes and dialyzed against HPLC water for 2 days. Purified N-type nanoparticles was then lyophilized.

3.3 Particle size and zeta potential

The particle size distribution and surface charge of B4F-linked HGC micelles was measured by Dynamic Light Scattering and zeta potential (NanoDLS Particle Size Analyzer, Brookhaven Instruments Corporation, Holtsville, NY). First lyophilized N-type and O-type nanoparticles were dissolved into HPLC water to prepare the 1 mg/mL solution. Then the solution was sonicated with a probe-type sonicator 3 times for 2 min each at 90 W to allow the micelles to self-assemble. To remove large aggregates, the solution was filtered with 0.8 μm and

0.2 μm syringe filters. The particle size measurements were taken in back scattering mode in triplicate at room temperature. The surface charge measurements were performed in a zeta dip cell. Particle size and surface charge values were expressed as mean ± standard deviation.

3.4 Cellular uptake study

Maintenance of the 4T1 breast cancer cell and delivery of the nanoparticles were done by Derek Rammelkamp (PhD student in Meng's group, Stony Brook University, NY).

Murine mammary carcinoma cells (4T1) were cultured in phenol red DMEM supplemented with 4.5 g/L D-Glucose, 1% of D-Glutamine, 1% of penicillin/streptomycin and 10% of fetal bovine serum at 37°C with a humidified 5% CO_2 atmosphere. Glass coverslips (12 mm diameter, Ted Pella Inc., Redding CA) sterilized by autoclaving were placed in the wells of a 24-well tissue culture plate (Corning Inc., Corning, NY) and 4T1 cells were seeded at a density of 7,500 cells/cm^2. The cells were then incubated with phenol red free and serum-free DMEM for 24 hours to allow the cells to adhere to the surfaces of the coverslips.

N-type and O-type nanoparticles were prepared in DMEM for delivery as follows. The B4F-linked HGC micelles conjugates were dissolved in DMEM (serum and phenol red-free) at a concentration of 300 μg/mL and probe-type sonicated 3 times at 90 W for 2 minutes each time, until the solution appeared homogenous. Then, the nanoparticle solution was sterile filtered with 0.8 μm syringe filter, followed by a 0.2 μm syringe filters to remove aggregates and biological contaminants. Afterwards, 500 μL of the nanoparticles solution was added to each well, and cells were incubated for 2 or 6 hours at 37°C and 95% relative humidity, with 5% CO_2. After

31

incubation, the cells were fixed with 3.7% formaldehyde for 15 minutes and permeabilized with 0.4% TritonX-100 for 8 minutes. F-actin was stained with 1:100 Alexa Fluor 546 (Thermo Fisher Scientific Inc., Pittsburgh, PA) for 20 minutes followed by two rinses with PBS. The glass coverslips were then transferred to a microscope slide and mounted with DAPI fluoromount-G. All samples were imaged with a confocal laser scanning microscope (Leica SP5, Leica, Buffalo Grove, IL).

Chapter 4: Results

4.1 O-type nanoparticles

4.1.1 Biotinylation efficiency of biotinylated nanomicelle

The biotinylation efficiency of biotinylated HGC (BHGC) was determined with HABA assay and summarized in Table 1. In order to disperse the hydrophobically modified nanoparticles in water, the solution was probe-type sonicated extensively (see Section 3.3), followed by water-bath sonication prior to the analysis. The biotinylation efficiency was defined in Equation 1-4 as the number of moles of biotin added in the reaction to the grafted biotin moieties per HGC molecule. When an HGC: biotin molar ratio of 1:107 was used, the average biotinylation efficiency was found to be 0.23%, which indicated that more than 99% of the biotin molecules failed to be conjugated to the HGC micelles.

HGC(mg)	Biotin(mg)	Molar ratio(GC:B)	Amount of Biotin per HGC	Biotinylation efficiency
100	11	1:107	0.25	0.23%

Table 1. Biotinylation efficiency of BHGC. Values represent the average of 3 measurements across from 3 independent experiments.

4.1.2 Binding of Biotin-4-Fluorescein (B4F)

To confirm that B4F was bound to avidinylated BHGC, the UV-vis absorbance spectroscopy of O-type nanoparticles in water solution was performed from 400 nm to 800 nm. The B4F contributed to a distinct emission peak at 482 nm (see Figure 11). In contrast, no absorbance peak was found for the unlabeled HGC micelles (Figure 12), indicating the presence of B4F in the solution.
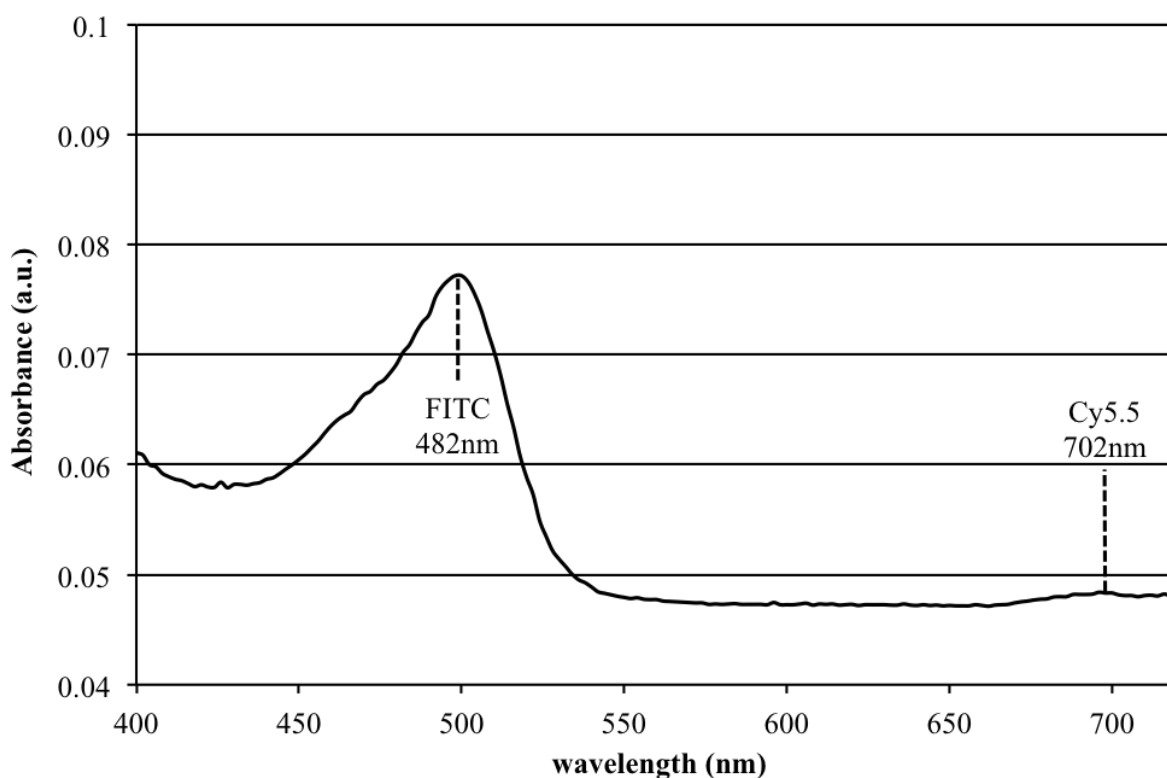
Figure 11. UV-vis spectrophotometric scan of O-type nanoparticles showing peaks corresponding to FITC (482 nm) and Cy5.5 (702 nm).
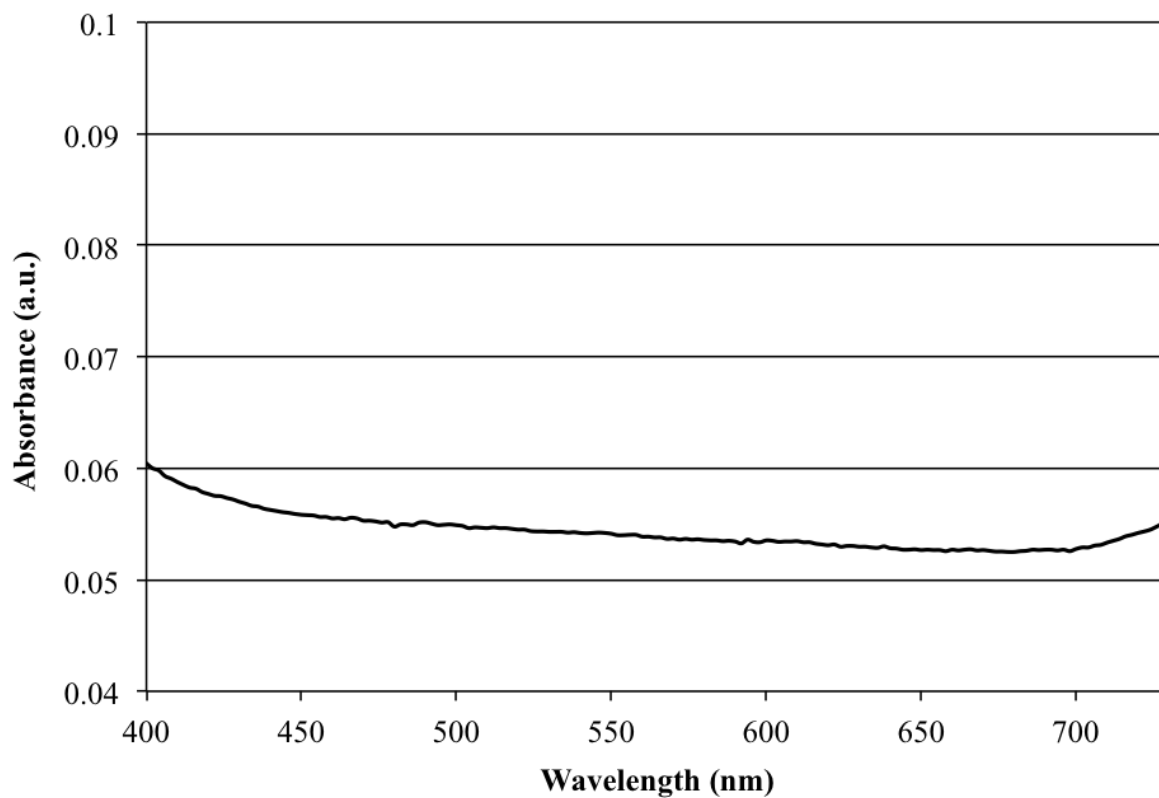
Figure 12. UV-vis spectrophotometric scan of HGC nanoparticles showing no peak.

4.1.3 Labeling of Cy5.5

The UV-vis spectrophotometric scan of O-type nanoparticles also showed a very weak peak at 702 nm (Figure 11), which is believed to be attributed by the Cy5.5 conjugated to the nanomicelle. No peak at 702 nm was found in the UV-vis spectroscopy data for the unlabeled HGC.

4.1.4 Size and surface charge of B4F-bound O-type nanoparticles

The hydrodynamic diameter and surface charge of O-type nanoparticles suspended in water was measured with DLS and zeta potential at room temperature in triplicate. The average diameter was 173.59±3.83 nm. The average surface charge was 11.96±1.24 mV. The representative size distribution profile is shown in Figure 13.
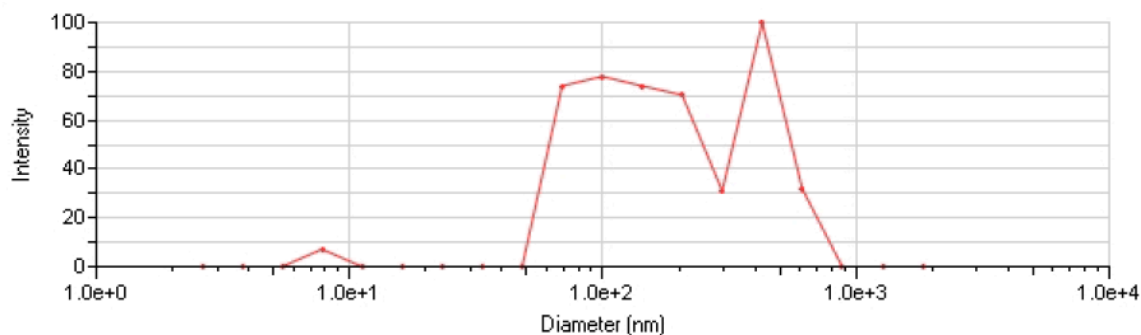
Figure 13. Size distribution profile of O-type nanoparticles. Data are representative of 3 measurements from a total of 3 experiments.

4.2 N-type nanoparticles

4.2.1 Biotinylation efficiency of biotinylated glycol chitosan (BGC)

Sulfo-NHS-LC-biotin was added to glycol chitosan to form biotinylated glycol chitosan (BGC) with the biotin: glycol chitosan molar ratios of 67:1 and 15:1. The biotinylation level of biotin (B) to glycol chitosan (GC) was determined by HABA assay and summarized in Table 2. The biotinylation efficiency was defined in Equation 1-4 as the number of biotin grafted on glycol chitosan molecule to the number of biotin added in the reaction. The biotinylation

efficiency of the first batch (B1) was 77%, which was 31% higher than the biotinylation efficiency of the second batch (46%).

Batch	GC(mg)	Biotin(mg)	Molar ratio(GC:B)	Biotin moieties per GC molecule	Biotinylation efficiency
B1	100	15	1:67	51.66	77.10%
B2	300	10	1:15	6.95	46.33%

Table 2. Biotinylation efficiency of BGC. Values represent the average and standard deviation of 3 measurements across from 3 independent experiments.

4.2.2 Biotin binding capacity of avidinylated BGC (BGC-A)

To ensure that enough biotin binding sites would be available for B4F added in subsequent steps, biotinylated glycol chitosan with relatively lower biotinylation level was preferred because there would be less competition for binding with avidin from other biotin moieties on the same BGC molecule. Hence, BGC with biotinylation efficiency of 46.33% (Batch B2) was chosen for the synthesis of BGC-A. One mole avidin was added to each mole of biotinlylated glycol chitosan via the interaction between avidin and biotin. The biotin binding density on the surface of BGC-A was analyzed with HABA assay and B4F quenching assay. According to the results obtained from HABA assay, each BGC-A molecule contained 0.88 biotin (B) moieties that were not bound to avidin added during synthesis. Additionally, results

from the HABA assay also showed that before adding avidin to BGC, total of ~7 (6.95) biotin molecules on each BGC particle were initially available for binding with avidin (see Table 2). Therefore, on average ~6 biotins per BGC molecule became bound to avidin. This result was unexpected since the avidin was added to BGC with a molar ratio of 1:1, giving a maximum binding capacity of 4 biotin molecules per BGC-A. The inconsistency could be attributed to the interaction between HABA dye and avidin molecules on BGC-A and therefore the HABA assay may not suitable for the avidinylated molecules. As a result, B4F quenching was further performed to characterize the biotin-binding capacity of BGC-A. The fluorescence-quenching assay was performed by titrating either the avidin standard solution or a solution of avidinylated BGC (BGC-A) with B4F.

Before titration, a serial dilution of B4F alone was prepared as the positive signal control to ensure the effectiveness of B4F. The representative titration profile is shown in Figure 14.
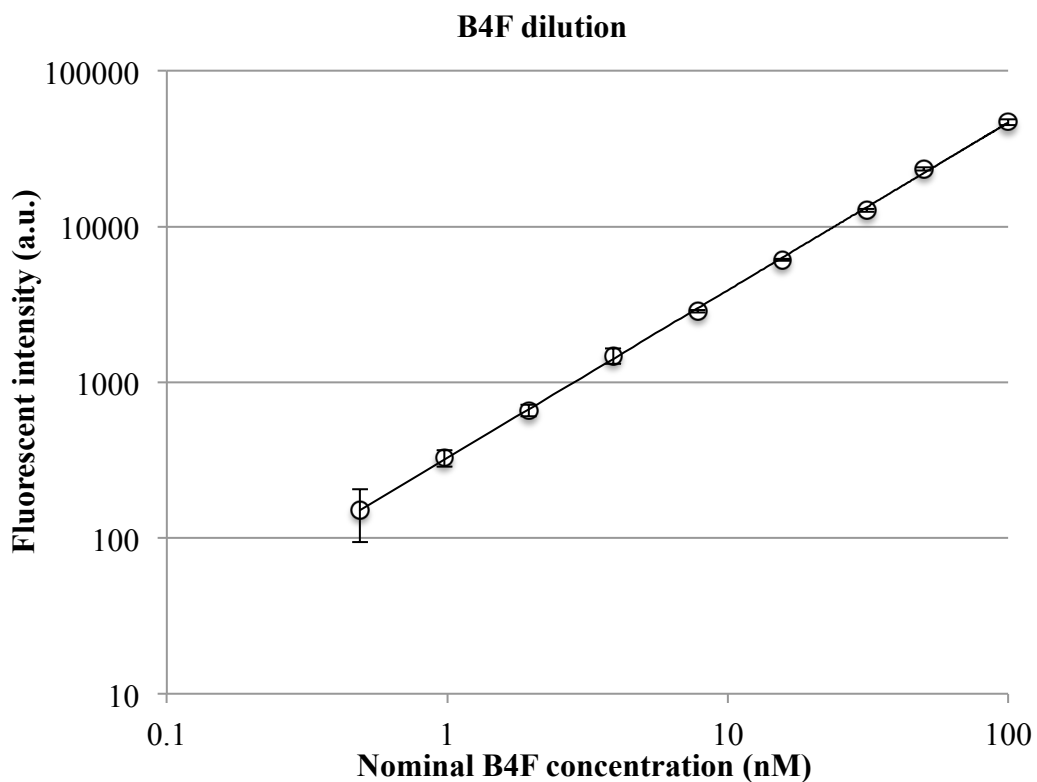
B4F dilution

Figure 14. Log-log titration profile of a 2-fold serial B4F dilution. The data points (open circle) fit a linear regression. Values represent the average and standard deviation of 3 measurements across from 3 independent experiments.

First to calibrate the biotin binding capacity of avidin alone, the concentration of avidin was determined by measuring the absorbance of avidin in water at 280 nm with a 1% extinction coefficient of 15.3 as provided by the manufacturer. [52] Then 0.73 nM of avidin was titrated with B4F with a nominal concentration up to100 nM. Representative titration profile of avidin is shown in Figure 15.

Figure 15. Log-log titration profile of 0.73 nM avidin. Values represent the average and standard deviation of 3 measurements across from 3 independent experiments. Regime I (open rectangle) at lower B4F concentration was fit to a second-order polynomial; regime II (open circle) at higher B4F concentration was fit to a linear model. The number of biotin-binding sites is determined by the point of intersection between two regimes, which is 5.2 as indicated by dotted line in the figure.

The first binding regime of B4F (open rectangles) to avidin was fit to a second-order polynomial and the second regime (open circles) was fit to a linear regression. Values represent the average and standard deviation of 3 measurements across from 3 independent experiments. The intersection point occurs at x=5.52, demonstrating the total 5.52 nM of biotin binding sites available in 0.73 nM avidin solution. The number of biotin binding sites on each avidin molecule is therefore obtained by dividing the total number of biotin binding sites (5.52 nmol) by the total number of avidin (0.73 nmol) in a 1 L sample, which is calculated to be 7.56.

Since each avidin molecule theoretically has a maximum of 4 biotin binding sites, [35] the value of biotin binding sites on each avidin molecule, 7.56, in terms of nominal B4F concentration, is divided by 4 to obtain a correction factor of 1.89 to get effective B4F concentration. As a result, the number of biotin binding sites per BGC-A molecule, in terms of effective B4F concentration, will be obtained by dividing the number of biotin binding sites obtained from the titration profile by the correction factor as shown in Equation 5.

$$effective\ binding\ sites = \frac{nominal\ binding\ sites}{correction\ factor} \qquad (5)$$

To determine the biotin binding capacity of BGC-A, 5 nM of BGC-A was titrated with B4F with a nominal concentration up to 100 nM and incubated for 1 hour at room temperature in the dark. Representative titration profile of BGC-A is shown in Figure 16.

BGC-A 5nM titration
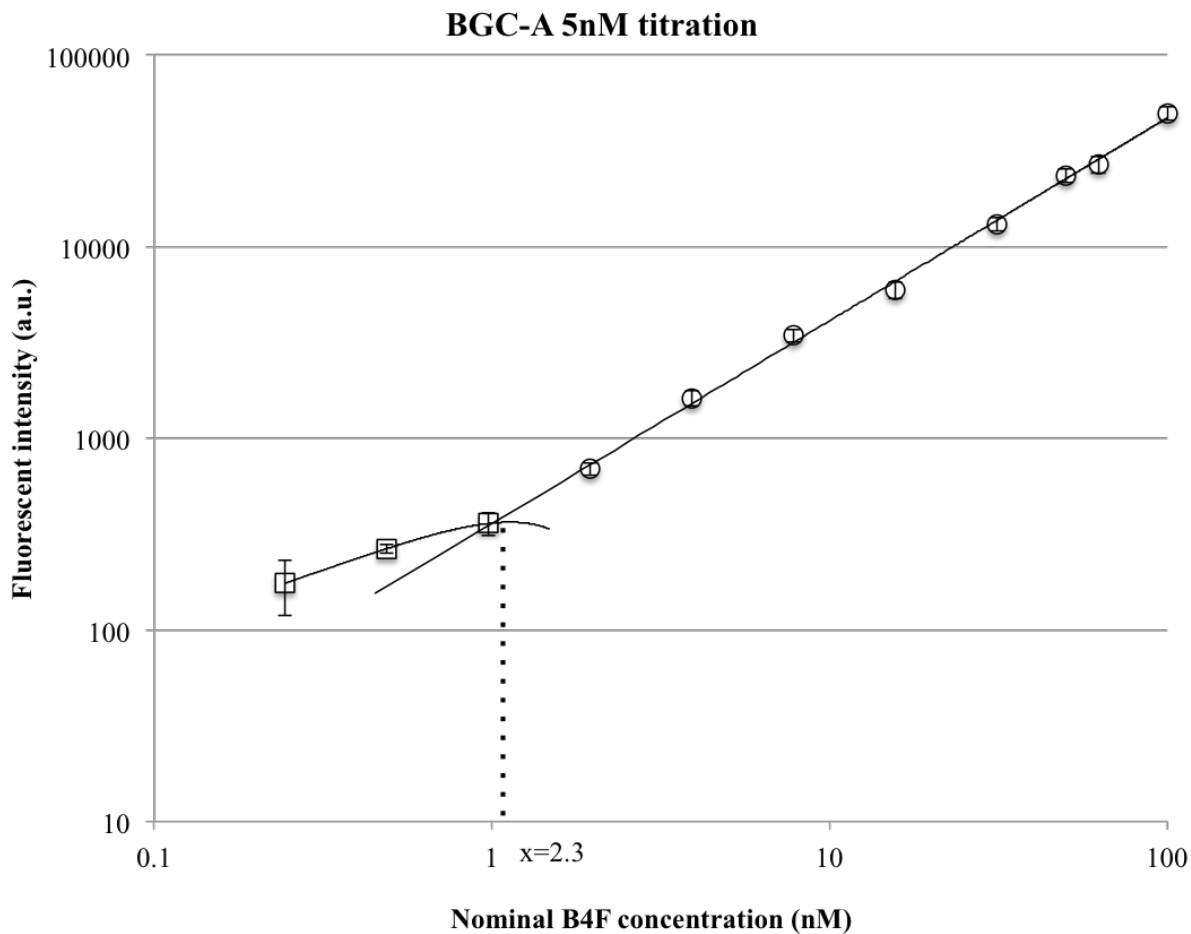
Figure 16. Representative titration profile of 5 nM BGC-A. Values represent the average and standard deviation of 3 measurements across from 3 independent experiments. Regime I (open rectangle) at lower B4F concentration was fit to a second-order polynomial; regime II (open circle) at higher B4F concentration was fit to a linear model. The number of biotin-binding sites is determined by the point of intersection, which is 2.3 as indicated by the dotted line in the figure.

The nominal x-intercept is 2.29 nM for 5 nM BGC-A. Therefore, the number of nominal

biotin binding sites on each BHGC-A particles is 0.46, which is obtained by dividing the total

biotin binding sites (2.29 nmol) by the number of BGC-A (5 nmol) in 1 L of sample. The number

of effective biotin binding therefore is 0.24 according to Equation 5.

One nM BGC titrated with B4F, as the control for zero biotin binding site, was included

and the titration profile is shown in Figure 17. The lack of nonlinear behavior in the data

demonstrated the inability of BGC to bind to B4F, which was expected because BGC did not
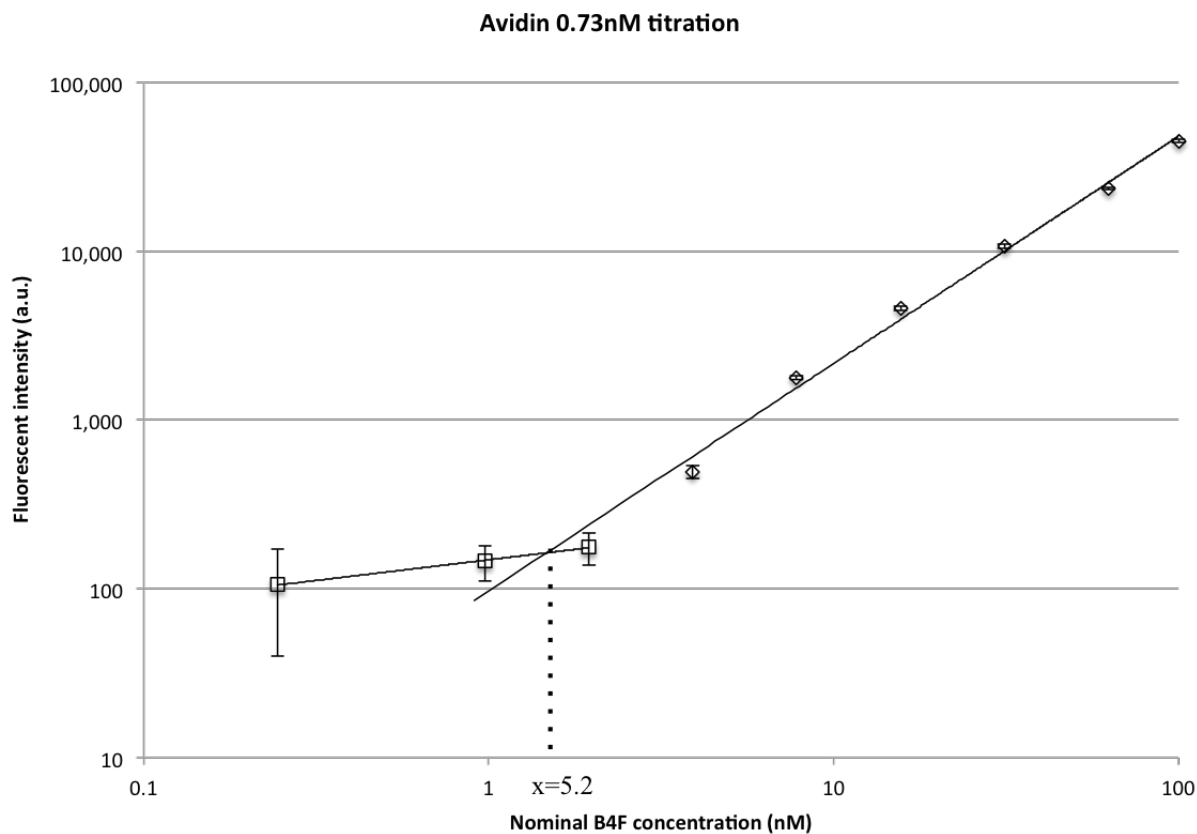
contain avidin.
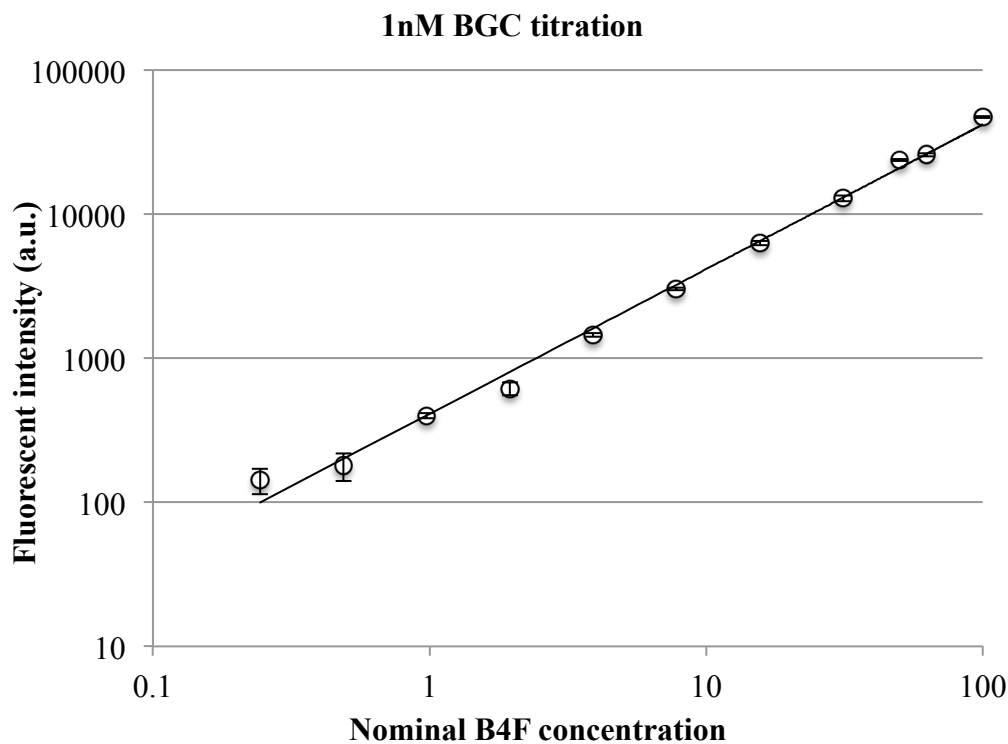
Figure 17. Titration profile of 1 nM BGC with B4F. Values represent the average and standard

deviation of 3 measurements across from 3 independent experiments. The data points (open

circle) fit to a linear regression.

4.2.3 Binding of B4F

In order to assist in the visualization of nanoparticles internalized in the cytoplasm, near-infrared dye Cy5.5 was added to N-type nanoparticles as described in Section 3.2.2.5. In addition, the biotin model molecule B4F emits at around 482 nm. As a result, the final product obtained after lyophilization exhibited a green appearance (see Figure 18). The conjugation of B4F was confirmed by UV-vis absorbance spectroscopy of an aqueous suspension of N-type nanoparticles (Tecan microplate reader). The emission peak at 482 nm was from B4F. The absorbance scanning profile for HGC micelles is shown in Figure 19. The absorbance scanning profile of HGC exhibiting no peak is shown in Figure 12, which indicates the existence of B4F in O-type nanoparticles.

Figure 18. Freeze-dried N-type nanoparticles.
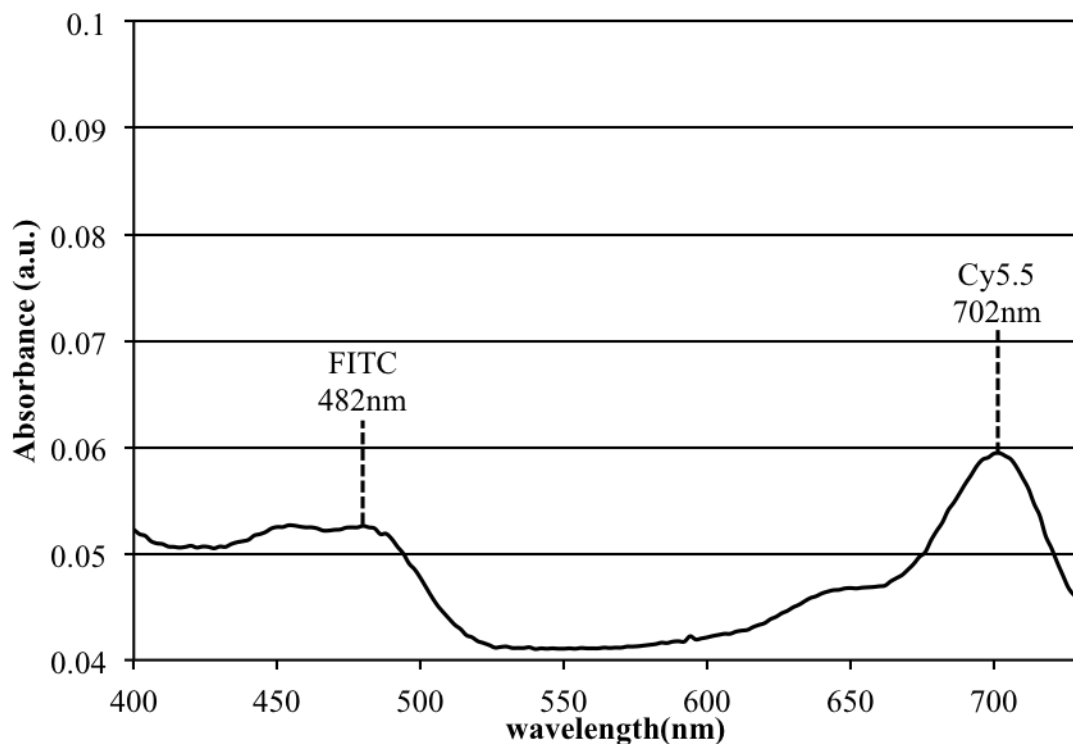
Figure 19. UV-vis spectrophotometric scan of N-type nanoparticles showing peaks

corresponding to FITC (482 nm) and Cy5.5 (702 nm).

4.2.4 Labeling of Cy5.5

The existence of Cy5.5 was confirmed by the peak at 702 nm in the UV-vis spectrophotometric scan of N-type nanoparticles (see Figure 19).

4.2.5 Size and surface charge (N-type nanoparticles)

The hydrodynamic diameter and surface charge of N-type nanoparticles in water was measured with DLS and zeta potential at room temperature. The average diameter was

197.89±6.39 nm. The size distribution profile is shown in Figure 20. The average zeta potential was 20.31±2.10 mV.
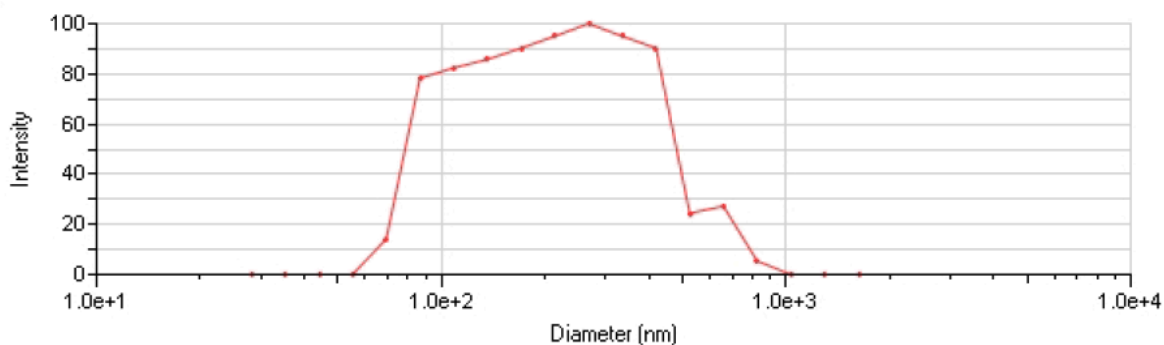
Figure 20. Size distribution profile of N-type nanoparticles. Data are representative of 3 measurements from a total of 3 experiments.

4.3 Delivery of nanoparticles to 4T1 breast carcinoma cells

A 500 μL suspension of either O-type or N-type nanoparticles prepared at a final concentration of 300 μg/mL in phenol red-free, serum-free DMEM solutions was added to 4T1 cells seeded in a 24-well tissue culture plate. The cells were incubated with the nanoparticle solutions for up to 6 hours before being rinsed, fixed and stained.

4.3.1 Uptake of O-type nanoparticles

The cellular uptake profile of O-type nanoparticles in 4T1 cells is shown in Figure 21(d)-(f) and Figure 22(d)-(f). The rapid cellular uptake of O-type nanoparticles was observed. Strong FITC signals and Cy5.5 signals were found inside the cells as green and red particles after 2

hours of incubation time (Figure 21 (d)-(f)). There was no obvious difference in fluorescence signals between the 4T1 cells incubated with O-type nanoparticles for 2 hours and 6 hours.

4.3.2 Uptake of N-type nanoparticles

The cellular uptake profile of N-type nanoparticles in 4T1 cells is shown in Figure 21(a)-(c) and Figure 22(a)-(c). The distribution of N-type nanoparticles appeared to be time dependent. After 2 hours of incubation time, a dim FITC signal was observed in the cytoplasm and there was barely any fluorescent signal from the Cy5.5 (Figure 21(a) and (b)). After 6 hours of treatment, both Cy5.5 and FITC fluorescence were visible (Figure 22(a)-(c)). Most nanoparticles were distributed evenly in the cytoplasm.
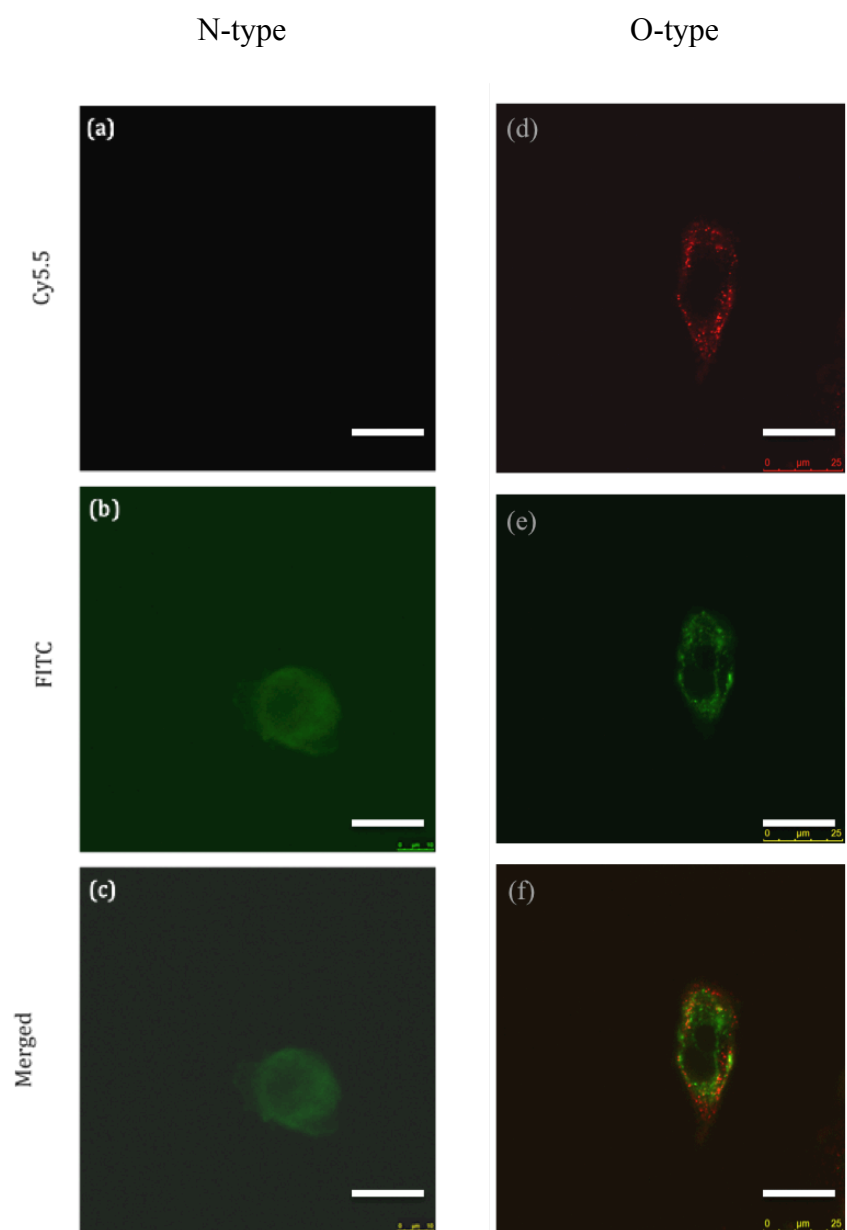
Figure 21. Confocal laser scanning microscope images of 4TI cells after incubation with N-type nanoparticles ((a)-(c)) and O-type nanoparticles ((d)-(f)) for 2 hours. For N-type nanoparticles, no Cy5.5 signal was observed after 2 hours of incubation time (a). Only a dim FITC signal was observed (b). For O-type nanoparticles, both red Cy5.5 and green B4F signals were visible (d)-(f). The red signals from Cy5.5 were observed after 6 hours in (d). The merged images were presented in (c) and (f). All scale bars are 25 μm.
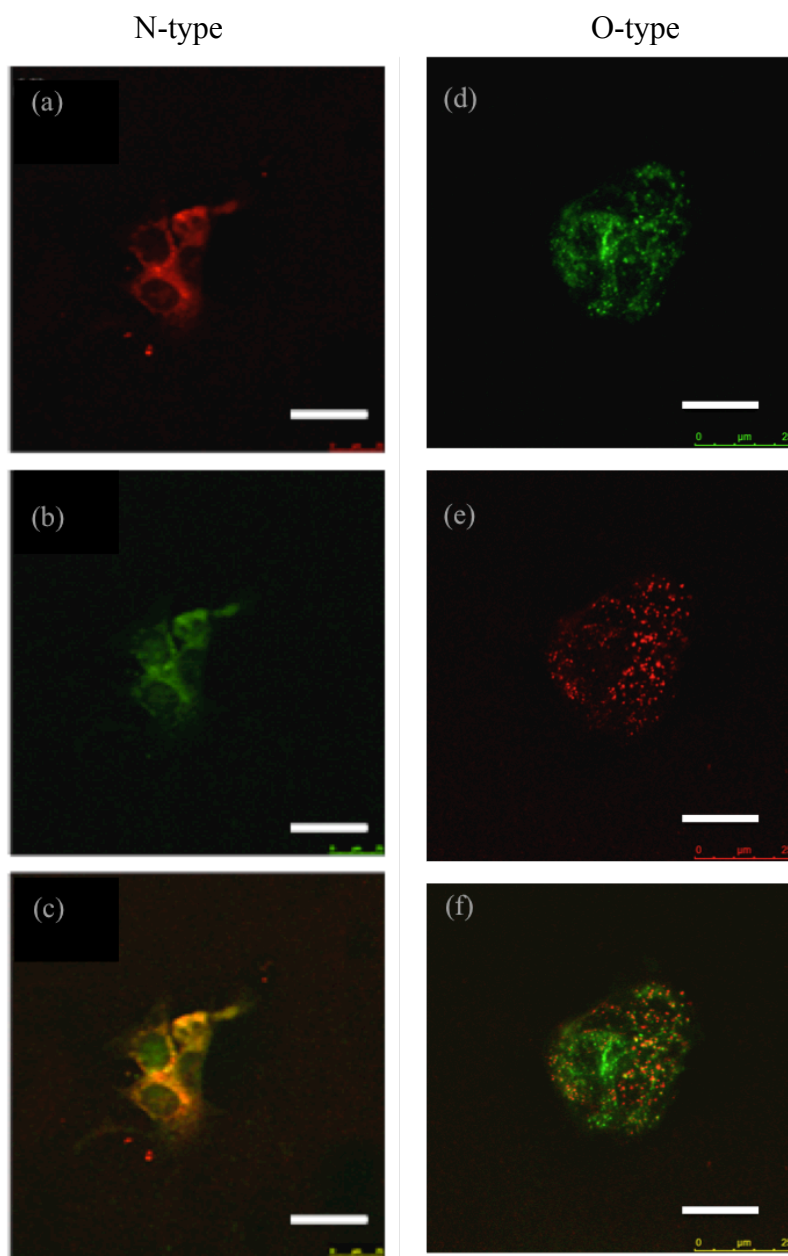
Figure 22. Confocal laser scanning microscope images of 4TI cells after incubation with N-type

nanoparticles ((a)-(c)) and O-type nanoparticles ((d)-(f)) for 6hrs. For N-type nanoparticles, red

Cy5.5 signal and green FITC signal from B4F were observed in (a) and (b). For O-type

nanoparticles, Cy5.5 and FITC signals were distributed evenly in the cytoplasm ((d) –(f)). The

merged images were presented in (c) and (f). All scale bars are 25 μm.

Chapter 5: Discussion

Traditional chemotherapy works by killing rapidly dividing cells with cytotoxic agents. However, besides cancer cells, many normal cells such as blood-forming cells in bone marrow, hair follicle cells and skin cells are proliferating fast as well. As a result, chemo drugs can damage healthy cells in human body and cause undesirable side effects. For example, up to 96% of patients undergoing cancer treatment experienced fatigue; [53] 70% to 80% of patients experienced nausea vomiting. [54] Moreover, serious side effects like neutropenia and gastrointestinal epithelial desquamation may increase the risk of infection, which can be life-threatening. [55]

In order to minimize the side effects of chemotherapy, targeted therapy has been developed. Generally speaking, a tumor-targeted drug delivery system contains tumor recognition agents that lead to tumor area. Therefore, cytotoxic drugs encapsulated or either conjugated to the system can be specifically released to cancer cells, resulting less damage to healthy cells and tissues. The glycol chitosan-based biotin-avidin linked micelle prepared in our study is a novel drug carrier model for specific drug delivery and controlled drug release.

5.1. Result of HABA assay

In our study, water-soluble glycol chitosan was hydrophobically modified and biotinylated via two different strategies. The main difference between the two strategies is whether micelle formation occurred before (O-type) or after (N-type) biotinylation. For N-type nanoparticles, Sulfo-NHS-LC-biotin was first conjugated to the amine groups at glycol chitosan.

Then avidin was added to form the BGC-A structure. The BGC-A molecule was further hydrophobically modified with 5β-cholanic acid. Finally, fluorescent dye Cy5.5 and model molecule B4F were added to BHGC-A. For O-type nanoparticles, D-(+)-biotin was added directly to the hydrophobically modified glycol chitosan nanomicelle via Steglich esterification with the presence of DCC and DMAP. Cy5.5 was added to fluorescently label the HGC nanomicelle. After that, avidin and B4F were added to BHGC with a molar ratio of 1:1:4 (avidin: BHGC: B4F) to obtain the B-A-B system.

The biotin conjugation efficiency of Sulfo-NHC-LC-biotin to glycol chitosan corresponded to the results reported in Hu's study in 2012. [56] Based on the result of HABA assay, the biotinylation efficiency of the Sulfo-NHS-LC-biotin conjugated to the glycol chitosan for N-type nanoparticles (46.33%) was significantly higher than the conjugation of biotin to HGC for O-type nanoparticles (0.23%). This large difference could probably be explained by the different solubility of these two types of nanoparticles. More specifically, the HABA assay was conducted in PBS buffer according to the manufacturer's instruction. [50] However, only the freeze-dried linear BGC polymer was soluble in PBS whereas the freeze-dried BHGC remained an insoluble suspension in PBS because the solubility of glycol chitosan in water is known to be 2 mg/mL [57] while the 5β-cholanic acid is immiscible in water. [58] It was therefore reasonable that biotinylated glycol chitosan (BGC) showed a greater solubility in water than the 5β-cholanic acid modified biotinylated glycol chitosan (BHGC). It was observed that precipitates remained in BHGC suspension even after extensive probe-type sonication. Those undissolved biotin molecules on the BHGC were unable to replace the HABA dye in the HABA/avidin premix. Consequently, the biotinylation level measured from the colorimetric assay might be lower than

the actual biotinylation level of BHGC. It could be concluded that HABA assay was restricted to water-soluble biotinylated compounds since the colorimetric assay was performed in water-based PBS media.

In order to further investigate the restriction of the commercial HABA assay, a new batch of Sulfo-NHS-LC-biotin linked glycol chitosan (BGC) was hydrophobically modified with 5β-cholanic acid as described in Section 3.2.1.1 and HABA assay was performed both on the water-soluble polymer BGC before hydrophobic modification and on the hydrophobically modified BGC. According to the results of HABA assay, each BGC molecule contained 11.29 biotin molecules (gave a biotinylation efficiency of 75.27%) prior to the addition of 5β-cholanic acid and after hydrophobic modification, it was estimated that there were 7.65 biotin molecules on each glycol chitosan (gave a biotinylation efficiency of 51.00%). Moreover, the hydrophobically modified conjugates solution was cloudy in water even after being probe-type sonicated for 3 times (2 mins each time). The discrepancy in HABA assay results before and after hydrophobic modification of BGC further demonstrated that the HABA assay could not be used to accurately determine the biotinylation level of water-insoluble biotinylated compounds. This could explain why the biotinylation level of BHGC (O-type) nanomicelles prepared in our study was unexpectedly low (0.23%) as the HABA assay was conducted after the nanomicelles were formed.

5.2 Result of fluorescence quenching assay

The HABA assay was limited to the determination of the biotinylation level of molecules that contained only biotin, and not avidin because both biotin and avidin contributed to the color change of the HABA dye. Therefore, this colorimetric assay would not give a reasonable result for the biotinylation level of BGC-A due to the interaction between avidin on BGC-A and HABA dye. HABA molecules that had already been replaced by biotin might bind to avidin on BGC-A with empty binding sites to re-form the yellow-orange colored avidin-HABA complex, which would generate an interfering signal. As a result, a B4F fluorescence quenching assay was performed to determine the biotin binding capacity of the avidinylated moiety (N-type BGC-A) based on the fact that B4F fluorescence quenches when binding to avidin or streptavidin.

The biotin binding capacity for BGC-A (N-type) showed that on average, each BGC-A molecule contains 0.24 empty sites, suggesting that every four BGC-A molecules would contribute 1 binding site available for the model molecule B4F. In other words, the avidin on BGC-A was almost saturated and there was little space for the B4F to occupy.

The O-type nanoparticles were not suitable for fluorescence quenching assay because avidin was added after the micelles were formed, and their solubility in water prevented accurate measurement.

5.3 Physicochemical properties of O-type and N-type nanoparticles

Both of the O-type and N-type nanoparticles were able to self-assemble to micelles in aqueous environment with diameters of 197.9±6.4 nm (N-type) and 173.6±3.8 nm (O-type). In

our previous study [59] it has been shown that the diameter of unlabeled HGC was 288.6±21.8 nm. In Li's study, [29] unlabeled HGC showed a diameter of 211±14 nm. The N-type nanoparticle was smaller than the plain HGC possibly because a different polymer to 5β-cholanic acid feed ratio was used. In Chin et al. study, 5β-cholanic acid was added to glycol chitosan polymer with the molar feed ratio of 0.185:1 (5β-cholanic acid: sugar residue on glycol chitosan). For the N-type nanoparticles developed in the current work, micelle formed after biotinylation and avidinylation of glycol chitosan. The molecular weight of BGC-A (probably around 320 kDa) was higher than GC (250 kDa) as the molecular weight of avidin is 66 kDa and the molecular weight of Sulfo-NHS-LC-biotin is 556.59 Da. As a result, when the same mass ratio of 5β-cholanic acid to polymer was used, the molar ratio of 5β-cholanic acid to sugar residues on BGC-A (~0.237) is higher than the molar ratio of 5β-cholanic acid to sugar residue on GC (0.185). The higher degree of substitution indicated a formation of a more compact hydrophobic core surrounded by hydrophilic shell, leading to a smaller size. [60] The relatively smaller size of O-type nanoparticles could be probably attributed to the conjugation of a water-insoluble biotin to the glycol portions on HGC. The glycol groups acted as hydrophilic polar shells when the micelles were formed. As result, upon the replacement of glycol groups with the hydrophobic biotins, the increase of hydrophobic to hydrophilic components ratio in a nanomicelle generated a large micelle. Further studies need to be done to exploit the different size of O-type and N-type nanoparticles. It can be noticed that both types of nanoparticles did not exhibit a single peak in the size distribution profiles, suggesting that the solution was a mixture of HGC-based micelles and unbound molecules. For example, the second peak around 8 nm shown in Figure 13 (size distribution profile of O-type nanoparticles) was most likely from the

unbound avidin protein. [61] The ratio of polymer to biotin and avidin molecules added can be re-designed to increase the monodispersity of the nanoparticles.

The surface charge of N-type and O-type nanoparticles was 20.3±2.1 mV and 12.0±1.2 mV, respectively. The surface charge of O-type nanoparticle was comparable to the surface charge of 13.2±0.2 mV for unlabeled HGC micelle reported before. [59] The positive surface charge of these two types of nanoparticles could be attributed to the presence of primary amine groups at chitosan main chain, which facilitates their interactions with negatively charged cancer cells membranes. [48] The N-type nanoparticles were more positive compared with either the O-type nanoparticles or the unlabeled HGC probably because the BGC (N-type nanoparticles) contained more biotin molecules than BHGC (O-type nanoparticles) and therefore avidin added to BGC had a greater opportunity to be attached by the biotins than avidin added to BHGC. As positively charged glycol proteins, [62] the addition of more avidin molecules likely contributed to an overall more positive surface charge.

5.4 Binding of B4F and labeling of Cy5.5

The absorbance spectra of the O-type and N-type nanoparticles prepared in water exhibited peaks at 484 nm and 707 nm, confirming the existence of B4F and Cy5.5 in both systems. Whereas, at the same concentration, O-type nanoparticles (0.077 a.u.) showed a 31.2 % higher absorbance at 484 nm than N-type did (0.053 a.u.), demonstrating that O-type nanoparticles owned a greater amount of B4F molecules than the N-type nanoparticles did. This result could be explained by the difference of biotin to avidin molecules molar ratio between O-type and N-type nanoparticles. During nanoparticle preparation, avidin was added to each type of

nanoparticles with the same molar ratio of 1:1 (avidin: nanoparticles), which linked to the biotin molecules existing on the surfaces of BGC (N-type) or BHGC (O-type). According to the results of HABA assay, per BHGC micelle had 0.25 biotin molecules while per BGC polymer had 6.95 biotin molecules. Therefore, the avidin added to N-type nanoparticles were more likely to get saturated by the biotin molecules on BGC polymer surface. In other words, it could be estimated that there were more biotin binding sites left on the surface of BHGC-A (O-type) than the BGC-A (N-type). According to the results from the B4F fluorescence quenching assay, there was only 0.24 binding site remained for B4F on each BGC polymer.

Then, when the same amount of B4F was added to O-type and N-type nanoparticles (molar ratio B4F: nanoparticle=4:1), B4F molecules added to O-type nanoparticles had a greater opportunity to bind to the empty sites on avidin, giving a higher signal at emission at 484 nm than the BGC-A (N-type). (see Figure 23)
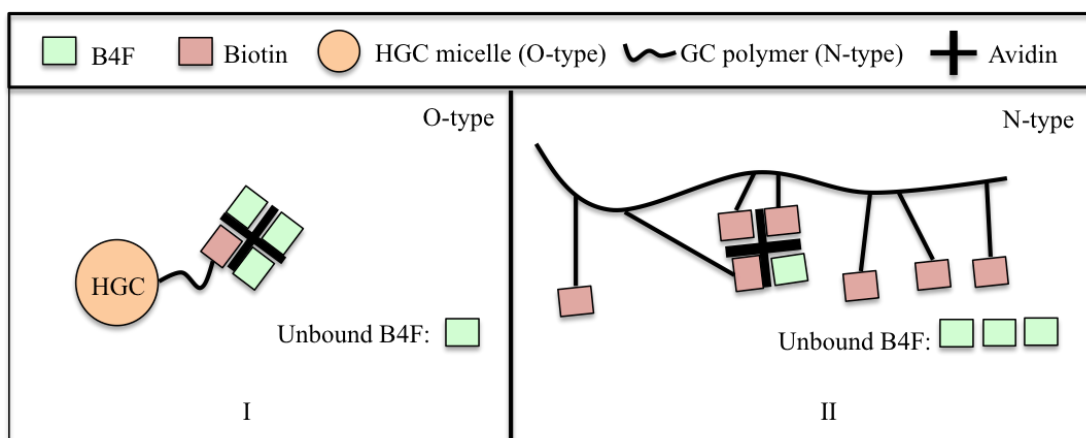
Figure 23. Schematic representation for binding of B4F. Suppose 1 avidin molecule was added to 1 BHGC (O-type) micelle (panel I) or 1 BGC (N-type) linear polymer (panel II). Then, 4 B4F molecules were added to each type of nanoparticle. As shown in the figure, BHGC contains less than 1 (0.25) biotin molecules so 3 of 4 B4F molecules could link to the 3 empty sites on avdin. BGC contains 7 biotin molecules and they occupied 3 binding sites on avidin (assumed) so only 1 B4F could link to the avidin and the other three would be removed by following dialysis. All drawings showed here are just rough estimates but not exact numbers.

5.5 Cellular uptake

Based on the fluorescence characterization of the nanoparticles, we expected the fluorescence signal from B4F and Cy5.5 to co-localize after cellular uptake. We examined this hypothesis by conducting a cellular uptake study using breast carcinoma cells. Under same incubation condition, 4T1 cells incubated with O-type nanoparticles showed a stronger FITC fluorescent signal than cells treated with N-type nanoparticles, indicating that O-type nanoparticles contained more B4F molecules. Co-localization of FITC and Cy5.5 signals was observed after 6 hours of treatments for both nanoparticles types (see Figure 21 (f) and Figure 22

(f)). It further confirmed the formation of HGC-based B-A-B structure and demonstrated that this system was stable in intracellular environment. Because of the high affinity of avidin to biotin molecules, the HGC-based nanoparticles are expected to be stable and functional over a wide range of pH and temperature in different environments.

As mentioned in section 1.4.5, both avidin and biotin exhibit certain tumor-targeting abilities. Avidin contains terminal *N*-acetylglucosame and mannose residues that are able to bind lectins. It has been found that lectins are expressed differently on normal and tumor cells. As a result, avidinylated molecules can be recognized by the lectins on the surface of tumor cells and therefore used as drug carries. [63] Besides, biotin receptors involved in the absorbance of vitamins by cells are found be overexpressed on the cancer cell surface as rapidly dividing cancer cells need sufficient nutrition. Thus, biotin can also be used as a tumor-targeting molecule to identify tumor cells. [64] So far, in this study it is hard to decide which factor plays a dominant role in the cellular uptake of nanoparticles in 4T1 cells while it can be concluded that the different cellular uptake abilities between N-type and O-type nanoparticles might be partly attributed to the different amounts of biotin and avidin molecules they contained. Further study is needed to figure out the cellular mechanism involved in the biotin-avidin modified nanoparticles uptake.

Chapter 6: Conclusion

HGC, as a cationic micellar polymer, has attracted increasing attention in recent decades and exhibits a great potential in a wide range of biomedical applications. In this study, HGC nanoparticles were modified with biotin through two different strategies where HGC molecules were biotinylated either at the amine groups ($-NH_2$) or the hydroxyl groups ($-OH$) on the chitosan backbone. Two types of HGC based biotin-avidin-biotin (B-A-B) systems were successfully achieved with particle diameters and surface charges ranging from 173.6 nm- 197.9 nm and 12.0 mV- 20.3 mV.

Biotin-4-fluorescein (B4F), as a model biomolecule, was linked to the biotinylated HGC via before the nanoparticles were delivered to breast cancer cells. Also, cyanine 5.5 was conjugated to HGC to aid in the visualization of delivered nanoparticles. Confocal microscope images showed that nanoparticles delivered at a concentration of 0.3 mg/mL were distributed widely throughout the cytoplasm of 4T1 mouse breast cancer cells after 6 hours of treatment. Furthermore, co-localization of the Cy5.5 and FITC signals demonstrated that B4F was successfully conjugated and stable in the intracellular environment.

This HGC-based B-A-B system is a flexible platform for drug delivery as B4F can be replaced by different biotinylated moieties to biofunctionalize the HGC-based drug delivery vehicle. For example, anti-cancer drugs like doxorubicin [65] or paclitaxel [66] have been successfully biotinylated and hence it is possible to delivery these drugs with the HGC-based BAB system. In addition, cell-specific recognition molecules could also be biotinylated and linked to the BAB system to lead the nanoparticles to tumor sites with higher specificity and

efficiency. As a result, the selectivity of the delivery system can be improved and the side effects due to the release of drugs in non-specific sites can be minimized. Taken together, the HGC-BAB nanoparticle is a potential candidate for drug delivery.

Chapter 7: Future work

Next, different ratios of biotin/avidin to polymer or nanomicelle will be tested to improve the physicochemical properties of biotin-avidin-biotin linked HGC based systems. NMR and TEM will be performed to further characterize the nanoparticles. To study the cellular distribution and cytotoxicity of O-type/N-type nanoparticles, cellular uptake study will be conducted in different cell lines with different nanoparticle concentrations.

Moreover, in order to improve the selectivity of the HGC-based B-A-B nanoparticles, next, we will incorporate biotinylated tumor-targeting reagents to biotinylated HGC via the biotin-avidin linkage. Nanoparticles will be delivered to both cancer cells and normal cells to investigate the tumor-selective ability.

Reference

1. D. Hanahan, R. A. Weinberg, The hallmarks of cancer, Cell, 100 (2000): 57-70.

2. American Cancer Society, Cancer facts & figures 2014, Atlanta: American Cancer Society, 2014.

3. G. H. Lyman et al., Risk of mortality in patients with cancer who experience febrile neutropenia, Cancer, 116 (2010): 5555-5563.

4. Y. A. Luqmani, Mechanisms of drug resistance in cancer chemotherapy, Med Princ Pract, 14 (2004): 35-48.

5. C. Holohan et al., Cancer drug resistance: an evolving paradigm, Nature Reviews Cancer, 13.10 (2013):714-726.

6. H. Maeda, J. Wu, T. Sawa, Y. Mastsumura, K. Hori, Tumor vascular permeability and the EFR effect in macromolecular therapeutics: a review, J. Contr. Rel, 65 (2000): 271-284.

7. Y. Wang et al., A nanoparticle-based strategy for the imaging of a broad range of tumours by nonlinear amplification of environment signals, Nature Materials, (2013).

8. S. A. Kulkarni , S. Feng, Effects of particle size and surface modification on cellular uptake and biodistribution of polymeric nanoparticles for drug delivery, Pharmaceutical research 30.10 (2013): 2512-2522.

9. A. Kumari, S. K. Yadav, S. C. Yadav, Biodegradable polymeric nanoparticles based drug delivery systems, Colloids and Surfaces B: Biointerfaces 75.1 (2010): 1-18.

10. J. R. Baker, Dendrimer-based nanoparticles for cancer therapy, ASH Education Program Book 2009.1 (2009): 708-719.

11. J. Conde, G. Doria, and P. Baptista, Noble metal nanoparticles applications in cancer, Journal of drug delivery, 2012 (2011).

12. K. T. Yong, et al, Preparation of quantum dot/drug nanoparticle formulations for traceable targeted delivery and therapy, (2012).

13. Y. Malam, M. Loizidou, A. M. Seifalian, Liposomes and nanoparticles: nanosized vehicles for drug delivery in cancer, Trends in pharmacological sciences, 30.11 (2009): 592-599.

14. R. Trivedi, U. B. Kompella, Nanomicellar formulations for sustained drug delivery: strategies and underlying principles, Nanomedicine, 5.3 (2010): 485-505.

15. M. C. Jones, J. C. Leroux, Polymeric micelles–a new generation of colloidal drug carriers, European journal of pharmaceutics and biopharmaceutics, 48.2 (1999): 101-111.

16. A. C. Miller et al., Block copolymer micelles as nanocontainer for controlled release of protein from biocompatible oil phase, Biomacromolecules, 10 (2009): 732-741.

17. M. L. Forrest et al., Paclitaxel prodrugs with sustained release and high solubility in poly(ethylene glycol)-*b*-(ε-caprolactone) micelle nanocarriers: pharmacokinetic disposition, tolerability, and cytotoxicity, Pharm. Res., 25 (2008).

18. E. Kobayashi, A. K. Iyer, F. J. Hornicek, M. M. Amiji, Z. Duan, Lipid-functionalized dextran nanosystems to overcome multidrug resistance in cancer, Clin. Orthop. Relat. Res., 471 (2013): 915-925.

19. M. Chopra, Synthesis and optimization of streptomycin loaded chitosan-alginate nanoparticles, International Journal of Scientific & Technology research, 1 (2012): 31-34.

20. J. Liu et al., Preparation of polymer-based multimodal imaging agent to visualize bone regeneration, J. Contr. Rel., 157 (2012): 398-405.

21. S. Dhawan, A. K. Singla, V.R.Sinha, Evaluation of mucoadhesive properties of chitosan microspheres prepared by different methods, AAPS Pharm. Sci. Tech., 5(2004).

22. J. Dutta, S. Tripathi, P.K. Dutta, Progress in antimicrobial activities of chitin, chitosan and its oligosaccharides: a systematic study needs for food applications, Food Sci. Tech., 2011.

23. R. Riva et al., Chitosan and chitosan derivatives in drug delivery and tissue engineering, Adv. Polym. Sci., 244 (2011): 19-44.

24. M. R. Huo et al., Synthesis and characterization of low-toxic amphiphilic chitosan derivatives and their application as micelle carrier for antitumor drug, International J. Phar 394 (2010): 162-173.

25. S. Kwon et al., Physicochemical Characteristics of self-assembled nanoparticles based in glycol chitosan bearing 5β-cholanic acid, Langmuir 19 (2003): 10188-10193.

26. A. Enhsen, W. Kramer, G. Wess, Bile acids in drug discovery, Drug Disov. Today, 3 (1998): 409-418.

27. J. H. Kim et al., Hydrophobically modified glycol chitosan nanoparticles as carriers for paclitaxel, J. Controlled Release, 111 (2006): 228-234.

28. K. H. Min et al., Hydrophobically modified glycol chitosan nanoparticles-encapsulated campthecin enhance the drug stability and tumor targeting in cancer therapy, J. Controlled Release, 127 (2008): 208-218.

29. T. S. Li et al., Use of glycol chitosan modified by 5β-cholanic acid nanoparticles for the sustained release of proteins during murine embryonic limb skeletogenesis, J. Controlled Release, 144 (2010): 101-108.

30. J. H. Park et al., Self-assembled nanoparticles based on glycol chitosan bearing 5β-cholanic acid for RGD peptide delivery, J. Controlled Release, 95 (2004): 579-588.

31. T. Kean, M. Thanou, Biodegradation, biodistribution and toxicity of chitosan, Advanced Drug Delivery Reviews, 62.1 (2010): 3-11.

32. S. Hirano, H. Seino, Y. Akiyama, I. Nonaka, Bio-compatibility of chitosan by oral and intravenous administrations, Proceedings of the ACS Division of Polymeric Materials: Science and Engineering, American Chemical Society, Los Angeles, California, 1998

33. Pierce, Avidin-Biotin Technical Handbook, Thermo Scientific, 2010.

34. Hayat, M. A., ed. Methods of Cancer Diagnosis, Therapy and Prognosis. Springer, 2010.

35. Hermanson, Greg T. Bioconjugate techniques. Academic press, 2013.

36. M. Tarrus et al., RGD-avidin-biotin pretargeting to αvβ3 integrin enhances the proapoptotic activity of TNFα related apoptosis inducing ligand (TRAIL), Apoptosis, 13 (2008): 225-235.

37. M. Darvishi, A. Nomani, M. Amini, M. A. Shokrgozar, R. Dinarvand, Novel biotinylated chitosan-graft-polyethyleneimine copolymer as a targeted non-viral vector for anti-EGF receptor siRNA delivery in cancer cells, Internation J. Phar., 456 (2013): 408-416.

38. J. Liu, L. Zhang, C. Wang, H. Xu, X. Zhao, Preparation and characterization of lectin-conjugated chitosan fluorescent nanoparticles, Molecular Biosystems, 6 (2010): 954-957.

39. G. Kada, K. Kaiser, F. Heinz, and Hermann J. Gruber, Accurate measurement of avidin and streptavidin in crude biofluids with a new, optimized biotin–fluorescein conjugate, Biochimica et Biophysica Acta (BBA)-General Subjects, 1427.1 (1999): 33-43.

40. H. J. Gruber, et al., Accurate titration of avidin and streptavidin with biotin–fluorophore conjugates in complex, colored biofluids., Biochimica et Biophysica Acta (BBA)-General Subjects, 1381.2 (1998): 203-212.

41. M. J. Waner, D. P. Mascotti, A simple spectrophotometric streptavidin-biotin binding assay utilizing biotin-4-fluorescein, J. Biochem. Biophys. Methods, 70 (2008): 873-877.

42. Li, Min, et al., Biotin-decorated fluorescent silica nanoparticles with aggregation-induced emission characteristics: fabrication, cytotoxicity and biological applications, Journal of Materials Chemistry B, 1.5 (2013): 676-684.

43. L. Bu, *Trans*-resveratrol loaded chitosan nanoparticles modified with biotin and avidin to target hepatic carcinoma, International J. Phar., 452 (2013): 355-362.

44. N. S. White, R. J. Errington, Fluorescence techniques for drug delivery research: theory and practice, Advanced drug delivery reviews, 57.1 (2005): 17-42.

45. O. V. Przhonska, et al., Two-photon absorption in near-IR conjugated molecules: design strategy and structure–property relations, Advanced Fluorescence Reporters in Chemistry and Biology I. Springer Berlin Heidelberg, 2010. 105-147.

46. V. Ntziachristos, C. Bremer, R. Weissleder, Fluorescence imaging with near infrared light: new technological advances that enable in vivo molecular imaging, Eur. Radiol., 13 (2003): 195-208.

47. K. Kim et al., Tumor-homing multifunctional nanoparticles for cancer theragnosis: Simultaneous diagnosis, drug delivery and therapeutic monitoring, J. Contr. Rel., 146 (2010): 219-227.

48. S. Y. Chae. M. Jang, and J.Nah, Influence of molecular weight on oral absorption of water soluble chitosans, Journal of controlled release, 102.2 (2005): 383-394.

49. A. Chin, (2013). Development of cy5.5-labeled hydrophobically modified glycol chitosan nanoparticles for protein delivery. M.S. Thesis. Stony Brook University: U.S.A

50. Product manuals for Pierce Biotin Quantitation Kit, product number 21329, Thermo Scientific, Inc., Pittsburgh, PA, USA.

51. R. Mittal, M. P. Bruchez, Biotin-4-fluorescein based fluorescence quenching assay for determination of biotin binding capacity of streptavidin conjugated quantum dots, Bioconjugate chemistry, 22.3 (2011): 362-368.

52. Product manuals for Avidin (from egg white), product number 43-4401, Life technologies, Inc., Grand Island, NY, USA.

53. C. J. Nelson, A. J. Roth, Y. Alici, Geriatric Psycho-Oncology: A Quick Reference on the Psychosocial Dimensions of Cancer Symptom Management, Oxford University Press, 2014.

54. R. M. Navari, Overview of the updated antiemetic guidelines for chemotherapy-induced nausea and vomiting, Chemotherapy, 20 (2007): 21.

55. V. MacDonald, Chemotherapy: managing side effects and safe handling, The Canadian Veterinary Journal, 50.6 (2009): 665.

56. W. Hu, et al., Use of biotinylated chitosan for substrate-mediated gene delivery, Bioconjugate chemistry, 23.8 (2012): 1587-1599.

57. Specification sheet for glycol chitosan, product number G7753, Sigma-Aldrich, Inc., St. Louis, Missouri, USA.

58. Material Safety Data Sheet for 5β-cholanic acid, product number sc-214342, Santa Cruz Biotechnology, Inc., Dallas, Texas, USA.

59. A. Chin, G. Suarato, Y. Meng, Evaluation of physiochemical characteristics of hydrophobically modified glycol cells chitosan nanoparticles and their biocompatibility in murine osteosarcoma and osteoblast–like cells, J. Nanotech. Smart Mater, 1 (2014): 1-7.

60. H. Y. Nam, et al., Cellular uptake mechanism and intracellular fate of hydrophobically modified glycol chitosan nanoparticles, Journal of Controlled Release, 135.3 (2009): 259-267.

61. J.B. Haun, et al., Bioorthogonal chemistry amplifies nanoparticle binding and enhances the sensitivity of cell detection, Nature nanotechnology 5.9 (2010): 660-665.

62. L. Almonte, L., E. Lopez-Elvira, A. M. Baró, Surface-Charge Differentiation of Streptavidin and Avidin by Atomic Force Microscopy–Force Spectroscopy, ChemPhysChem, 15.13 (2014): 2768-2773.

63. Z. Yao, et al., Avidin targeting of intraperitoneal tumor xenografts, Journal of the National Cancer Institute, 90.1 (1998): 25-29.

64. Ojima, Iwao, Guided molecular missiles for tumor-targeting chemotherapy—case studies using the second-generation taxoids as warheads, Accounts of chemical research, 41.1 (2007): 108-119.

65. Allart, Brigitte, et al., A stable bis-allyloxycarbonyl biotin aldehyde derivative for biotinylation via reductive alkylation: application to the synthesis of a biotinylated doxorubicin derivative., Bioconjugate chemistry, 14.1 (2003): 187-194.

66. Lis, Lev G., et al., Synthesis and Biological Evaluation of a Biotinylated Paclitaxel with an Extra-Long Chain Spacer Arm., ACS medicinal chemistry letters, 3.9 (2012): 745-748.